High Redshift Quasars

The papers appended here summarize the work completed on this project during the referenced period.

NASA Grant NAG5-2563

Annual and Final Reports

For the Period 1 April 1994 through 30 September 1996

Principal Investigator
Dr. Martin S. Elvis

September 1996

Prepared for:

National Aeronautics and Space Administration
Goddard Space Flight Center
Greenbelt, Maryland 20771

Smithsonian Institution
Astrophysical Observatory
Cambridge, Massachusetts 02138

The Smithsonian Astrophysical Observatory
is a member of the
Harvard-Smithsonian Center for Astrophysics

The NASA Technical Officer for this grant is Dr. Nicholas White, Code 668, Laboratory **for High Energy Astrophysics**, NASA/Goddard Space Flight Center, Greenbelt, Maryland **20771.**

Associated Absorption at Low and High Redshift

Martin Elvis[1], Smita Mathur[1], Belinda Wilkes[1], Fabrizio Fiore[1,2], Paolo Giommi[2] & Paolo Padovani[2]

1: Harvard-Smithsonian Center for Astrophysics, 60 Garden St., Cambridge, MA 02138, USA
2: SAX Data Center, Roma, Italy

Abstract.

1. Introduction

Combining information on absorbing material in AGN from X-ray and the UV creates a powerful investigative tool. Here we give examples from both low and high redshift.

At low redshift we have found that the ionized ("warm") X-ray absorbers and the associated UV absorbers in two radio-loud quasars were due to the same material : an X-ray quiet quasar 3C351 (Fiore et al., 1993, Mathur et al. 1994) and a red quasar 3C212 (Elvis et al., 1994, Mathur 1994). In both cases the absorber is situated outside the broad emission line region (BELR), is outflowing, and is highly ionized. This delineates a new nuclear component in lobe-dominated radio-loud quasars. Could the same component explain all the X-ray and UV absorption in AGN seen over the past 20 years and more (Anderson 1974, X-RAY REF, Ulrich 1988)?

We have recently tested this generalization using the best studied of all AGN, NGC5548. We applied the same photoionization modeling method (Mathur et al., 1994) to the X-ray and UV absorbers in NGC5548 to determine whether consistent values for the abundances of all the observed ions could be obtained. In NGC5548 the model must meet two extra requirements: it must not lead to a density for the absorber in conflict with its recombination time; and the distance of the absorber from the continuum source must not conflict with the well-determined BELR size.

At high redshifts X-ray absorption and rest frame UV absorption have been found together in a number of radio-loud quasars. The low energy X-ray cut-offs in these objects are likely to be due to their environment. The absorption seen in the high-z quasars may be similar to the low-Z 'X/UV' absorption, but on a larger scale.

2. Testing the X/UV models with NGC5548

ASCA observations confirm the presence of an ionized absorber in NGC5548 with equivalent $N_H = 3.8 \times 10^{21} cm^{-2}$ (Fabian et al. 1994a), and resolving the OVII and OVIII absorption edges. An Fe-K edge is not detected ($\tau_{Fe-K} \leq 0.1$).

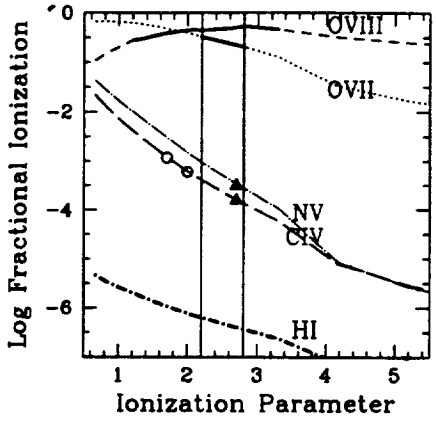

Figure 1. Ionization fractions of OVII, OVIII, CIV, NV and HI as a function of U. The thick lines mark the observed ranges for OVII and OVIII (ASCA). Triangle: HST values for CIV and NV; o: IUE range. The HST range for HI is large (see text) represented by the thick curve. The vertical lines define the best fit model parameter: $2.2 < U < 2.8$.

HST finds blueshifted UV absorption lines (Korista et al. 1995). The CIV and N V doublets, and an associated Lyα absorption line ($N_{HI} \geq 4 \times 10^{13}$ cm^{-2}) are all clearly seen in the mean FOS spectrum.

We searched (using CLOUDY, Ferland 1991) for a photoionized absorber satisfying both X-ray and UV constraints. Figure 1 shows the ionization fractions of OVII and OVIII as a function of ionization parameter, U. We used the de-reddened continuum for NGC5548 and assuming solar abundances (Grevesse & Andres 1989) and density $n = 10^7$ atoms cm^{-3}. The ASCA constraints on the fractional ionization of OVII and OVIII (Fig.1, thick lines) allow only a narrow range of U, $2.2 < U < 2.8$.

In the mean HST spectrum, the CIV doublet ratio is 3.8±0.2, putting them off the linear portion of the curve of growth (see e.g. Spitzer 1978, Weise et al. 1966). A consistent solution for all three ions, CIV, NV and HI is obtained for b=40 km s^{-1}, with only a small tolerance for both UV and X-ray constraints to be met (see Mathur et al. 1995 for the details of the model). The matching of the five ion abundances leads us to conclude that the UV and X-ray absorbers in NGC5548 are one and the same.

An additional test of the model is now available. The HST Ly-α HI column density is highly uncertain: $13 < logN_{HI} < 18$, while the model values are tightly constrained, from 15.2 to 15.4. Mathur et al. (1995) noted that a Lyman edge absorption would be observed if $logN_{HI} > 16.3$, and would be detectable by HUT. In the event HUT did not find a Lyman edge (Kriss et al., these proceedings), implying $N_{HI} < 10^{\sim 16.3}$, close to our best fit value. This strengthens our X/UV model. OVI absorption would provide another strong test. Unfortunately the HUT spectrum seems to have low s/n in OVI, although the OVI absorption doublets may be present.

Our model is also consistent with the ASCA limit on an Fe-K X-ray absorption edge of $\tau < 0.1$, implying $N_{FeXVII} < 2 \times 10^{18}$ cm^{-2} (for solar abundance). For our best fit model the dominant stage of iron is FeXVII. (This is common. FeXVII dominates over a wider range of U than other ionization states since it is neon-like and so more stable than other iron ions.) We find $\log f_{FeXVII} = -0.77$, implying $N_{FeXVII} = 3 \times 10^{16}$, far below the ASCA limit.

The absence of an Fe-K absorption edge affects another model. The warm gas above and below the torus that electron scatters and polarizes light from the BELR into our line of sight in many Seyfert 2 galaxies is a natural candidate for the ionized X/UV absorbers (Krolik & Kriss, 1995). In unified schemes this gas will be seen pole-on in Seyfert 1 galaxies and will cause absorption. Krolik & Kriss (1995) predict an Fe-K or an Fe-L edge of optical depth ≥ 0.1. The absence of these features in the NGC5548 ASCA spectrum pushes these models to higher U and so lower n_e and larger size. Our X/UV absorber modeling finds smaller column density material at a lower ionization state, and so is due to some other nuclear component.

Netzer (1996) has modeled X-ray absorbers in a similar way to Mathur et al. (1995) but predicts that the UV lines will show N(NV)>N(CIV), in contradiction to the observations. He concludes that two separate absorbers are needed in NGC5548. However, Netzer uses a steep EUV slope ($\alpha \sim 6$ [???]). The observed continuum of NGC5548 instead has $\alpha \sim 2$ [???]. Mathur et al. (1994) noted the importance of using the actual continuum of the object being modeled. When this is done for NGC5548 N(NV)<N(CIV) (Mathur et al., 1995). This illustrates the danger of comparing results using differing assumptions.

Our model, together with the reverberation mapping variability constraints, leads us to understand the physical properties of the absorber. The absorber is highly ionized ($2.2 < U < 2.8$), has high column density ($N_H = 3.8 \times 10^{21}$ cm^{-2}), low density ($5 \times 10^5 t_4^{-1} < n < 5 \times 10^9$ cm^{-3}), and is situated outside the CIV emitting region ($2 \times 10^{16} < r_{abs} < 2 \times 10^{18}$ cm). The gas is outflowing with a mean velocity of 1200 ± 200 $km\ s^{-1}$ (relative to the host, Heckman 1978), and has a corresponding kinetic luminosity of $\sim 10^{43} ergs^{-1}$. A scenario in which the absorbing material comes off a disk, and is accelerated by the radiation pressure of the continuum source may explain the observed properties of the absorber.

We can now generalize our unification of UV and X-ray absorbing outflows from the lobe dominated radio-loud quasars to include radio-quiet Seyfert galaxies. This may also provide a link to the radio-quiet BALQSOs, which show unexpectedly strong X-ray absorption (Mathur, Elvis & Singh 1996, Green & Mathur [??] 1996). This analogy suggests that the UV/X-ray absorbers in radio-quiet AGN may be viewed close to edge-on, which would be a valuable known parameter if it can be independently supported.

3. Absorption in High-Z Quasars

A few ROSAT PSPC spectra of high redshift (z$\sim$3) quasars showed strong low energy cut-offs, suggesting strong obscuration (Elvis et al., 1994). A search of the whole PSPC pointed archive (Fiore et al., 1996) has now shown that only radio-loud quasars have X-ray colors (P=1%) suggesting cut-offs; so *low energy X-ray cut-offs are associated with the quasars*, and not with intervening systems

(since those would affect radio-quiet and radio-loud equally). Moreover, among radio-loud quasars those at high redshift are more cut-off than those at low z (P=0.04%); so *the X-ray cut-offs show evolution with cosmic epoch.*

Investigating the optical and radio properties of the 11 quasars with ROSAT cut-offs (Elvis et al., 1996) we find that *all* have associated absorption lines in their optical/ultraviolet spectra and/or show reddening associated with the quasar. We conclude that *absorption is highly likely to be the cause of the X-ray cut-offs* too. The implied X-ray column densities are a few$\times 10^{22}$ cm^{-2}.

Moreover, the higher redshift quasars are Gigahertz Peaked Spectrum source candidates suggesting that the absorbing material is extended on the scale of the radio sources (i.e. pc - kpc).

There are several trends within the sample: going from low to high redshift and luminosity we find a related change from low to high ionization, and from low to high compactness (as indicated by radio size and cut-off frequency). Interestingly, the ionization parameter and column densities are similar to those expected from a large 'cooling flow' ionized by a quasar. Even these pressures are insufficient to thermally confine the radio sources, but ram pressure can slow down their expansion. The suggestive picture that emerges is of radio sources that are both young and frustrated (Fanti 1990) by a high pressure surrounding medium.

Acknowledgments. BJW gratefully acknowledges the financial support of NASA contract NAS8-39073 (ASC) and SM of NASA grant NAGW-4490 (LTSA), and ME of NASA grant NAG5-1356 (ROSAT).

References

Anderson K.S., 1974, Ap.J., 189, 195.

Elvis M., Fiore F., Wilkes B.J., McDowell J.C., & Bechtold J., 1994, Ap.J., 425, 103.

Elvis M., Fiore F., Giommi P., & Padovani G., 1996, in preparation.

Fanti R., 1990, in "CSS & GPS Radio Sources" eds. C.Fanti, R. Fanti, C.P. O'Dea and R.T. Schillizi. [CNR, Bologna] Ferland, G. F. 1991 "HAZY", OSU Astronomy Department Internal Report.

Fiore F., Elvis M., Mathur S., Wilkes B.J., & McDowell J.C., 1993, Ap.J., 415, 129.

Fiore F., Elvis M., Giommi P., & Padovani G., 1996, in preparation.

Green P. & Mathur S., 1996, Ap.J., 462, 637.

Heckman T.M., 1978, PASP, 90, 241.

Kriss, G. et al. 1996, these proceedings.

Mathur, S., Wilkes, B., Elvis, M. & Fiore, F. 1994, ApJ, 434, 493

Mathur, S., Elvis, M. & Wilkes, B. 1995, ApJ, 452, 230

Mathur S., Elvis M., & Singh K.P., 1996, Ap.J.Letters, 455, L9.

Netzer H., 1996, preprint Tel Aviv Univ.

THE ASTROPHYSICAL JOURNAL, 455:L9–L12, 1995 December 10

STRONG X-RAY ABSORPTION IN A BROAD ABSORPTION LINE QUASAR: PHL 5200

SMITA MATHUR[1] AND MARTIN ELVIS
Harvard-Smithsonian Center for Astrophysics, 60 Garden Street, Cambridge, MA 02138
AND
K. P. SINGH[2]
Laboratory for High Energy Astrophysics, Code 668, NASA/GSFC, Greenbelt, MD 20771
Received 1995 September 5; accepted 1995 September 26

ABSTRACT

We present *ASCA* observations of the $z = 1.98$ prototype broad absorption line quasar (BALQSO): PHL 5200. The source was detected in both SIS and GIS. A power-law spectrum ($\alpha_E = 0.6^{+0.9}_{-0.6}$) with large intrinsic absorption ($N_H = 1.3^{+2.3}_{-1.1} \times 10^{23}$ cm^{-2}) best describes the spectrum. Excess column density over the local Galactic value is required at the 99% confidence level. This detection suggests that, although BALQSOs are X-ray–quiet, it is strong absorption in the BAL region that makes them appear faint to low-energy X-ray experiments. The required intrinsic absorbing column density is 2–3 orders of magnitude larger than earlier estimates of column densities in BALQSOs. This implies that the BAL systems are much more highly ionized than was previously thought.

Subject headings: quasars: absorption lines — quasars: individual (PHL 5200) — X-rays: galaxies

1. INTRODUCTION

Associated absorption is common in the optical and ultraviolet spectra of quasars (Ulrich 1988). A subset of these have very broad absorption line profiles extending up to $\Delta v = 0.1c$–$0.2c$ redward with respect to the quasar rest frame (see, e.g., Turnshek 1988). These broad absorption line quasars (BALQSOs) show absorption features due to high-ionization lines of C^{+3}, Si^{+3}, and other ions. Low-ionization BALQSOs have also been observed which show Mg^{+1} and/or Al^{+2} absorption troughs. BALQSOs have been estimated to have column densities $N_H \sim 10^{20}$–10^{21} cm^{-2} (Turnshek 1984; Hamann, Korista, & Morris 1993). As a class, BALQSOs share some common properties: they are always radio-quiet (Stocke et al. 1992), may have abundances 10–100 times solar (in their emission lines; Turnshek 1988, Hamann & Ferland 1993), and are X-ray–quiet (Green et al. 1995). Recent work suggests that BALQSOs are normal radio-quiet quasars seen from an unusual direction (Weymann et al. 1991; Hamann et al. 1993). In this case all radio-quiet quasars have collimated BAL outflows, which, however, are pointed out of our line of sight in some 90% of cases. Thus BALQSOs, far from being exotic objects, give us a special probe into the gasdynamics around the typical quasar.

However, physical conditions in the absorbing gas in the BALQSOs are poorly determined from optical/UV absorption-line studies (Lanzetta et al. 1991). This is because only a few, usually saturated, lines are measured, yielding lower limits to column densities for a few ions but little information on the ionization state. If, as in the narrow-line–associated absorbers, there is X-ray absorption as well as optical and UV, then the combined X-ray and UV analysis would allow us to derive the physical conditions in BALQSO absorption systems (Mathur et al. 1994; Mathur 1994; Mathur, Elvis, & Wilkes 1995). This, however, has been difficult, since BALQSOs are elusive X-ray sources and so are otherwise essentially unconstrained in their X-ray properties. In a soft X-ray study of quasars with *Einstein*, only four out of nine BALQSOs were detected (Zamorani et al. 1981). Initial results from *ROSAT* are mainly upper limits (Kopko, Turnshek, & Espey 1993; Green et al. 1995), implying that they are relatively faint in soft X-rays (i.e., have steep α_{ox}). Our understanding of BALQSOs is incomplete without a knowledge of their X-ray properties. In fact, lack of knowledge of the underlying ionizing continuum is one of the major uncertainties in the models of BALQSOs: Are they intrinsically X-ray–quiet (i.e., large α_{ox})? Or is it strong absorption that makes them look faint?

PHL 5200, a prototype BALQSO at $z = 1.98$ (Burbidge 1968), was detected in hard X-rays by the *EXOSAT* medium-energy (ME) experiment but not by the low-energy (LE) experiment (Singh, Westergaard, & Schnopper 1987). To obtain consistency between the *EXOSAT* ME and LE requires a column density of $\geq 10^{22}$ atoms cm^{-2}, making it an excellent candidate for examining the BAL region. We observed PHL 5200 with *ASCA* with this aim in mind. *Einstein* did not detect (Zamorani et al. 1981) and *ROSAT* has not observed PHL 5200.

2. *ASCA* OBSERVATIONS AND DATA ANALYSIS

ASCA (Tanaka et al. 1994) observed PHL 5200 on 1994 June 21 for a net exposure time of 17.7 ks (Table 1). *ASCA* has two solid-state imaging spectrometers (SIS0 and SIS1; Loewenstein & Isobe 1992) and two gas imaging spectrometers (GIS3 and GIS4; Ohashi et al. 1991). The SISs were operated in 2 CCD mode (see Fig. 1). The source was faint but was clearly detected in SIS0 and GIS3 (Fig. 1). The X-ray position from SIS0 is (J2000) $22^h28^m26^s$, $-5°18'54''$, 1.'1 from the optical position (Schneider et al. 1992), consistent with the current satellite pointing uncertainties (Tanaka et al. 1994). The source was off-axis in SIS1 (where it lay close to the gap between two chips) and GIS2 and was not detected in either. This is consistent with the fact that the optical axes of

[1] smita@cfa.harvard.edu.
[2] NRC Senior Research Associate, on leave from Tata Institute of Fundamental Research, Bombay, India.

TABLE 1

ASCA OBSERVATIONS OF PHL 5200

Instrument	Total Counts	Exposure (s)	Net Count Rate (s^{-1})
SIS0.....	513	16,587	0.01 ± 0.001
GIS3	505	16,788	0.006 ± 0.001

telescopes containing SIS0 and GIS3 are much closer to each other than the others. No other sources were seen in any of the instruments to a level similar to the count rates of PHL 5200.

Data were extracted in a standard way using the FTOOLS and XSELECT software.[3] Standard screening criteria were used as recommended in the *ASCA* ABC guide: a greater than 10° bright Earth angle, and a cutoff rigidity greater than 6 GeV/*c*. Hot and flickering pixels were removed from the SIS data using XSELECT. All SIS events of grade 0, 2, 3, and 4 were accepted. Data of both faint and bright modes with high, medium, and low telemetry rates were combined. These data can be combined without any calibration compromises. The *ASCA* X-ray telescope has a broad point-spread function, and jittering of the spacecraft can appear on arcminute scales. To take this into account, source counts were extracted from a circular region of 6′ radius for GIS3 and from a 4′ radius for SIS0. The source was pointed at the center of chip 1 of SIS0, putting the bulk of its photons into just one chip. Detectors SIS0 and GIS3 yielded ~500 total counts each. Data from these detectors cannot be combined, since the detectors have different properties. The background was estimated using the same spatial filter on the deep field background images (*ASCA* ABC guide). A background-subtracted count rate of $(1.04 \pm 0.15) \times 10^{-2}$ was observed by SIS0, and $(6.26 \pm 1.47) \times 10^{-3}$ by GIS3. The data were grouped to contain at least 10 counts (background-subtracted) per pulse-height analysis (PHA) channel to allow the use of the Gaussian statistic. The data have modest signal-to-noise ratio; however, it can be clearly seen that that there are essentially no counts below ~1 keV (~3 keV in the rest frame) (see Fig. 2). The highest rest energy detected for PHL 5200 is 12 keV at 3 σ for 0.5 keV wide bins. Figure 2 shows the SIS and GIS spectra of PHL 5200.

[3] FTOOLS is a collection of utility programs to create, examine, or modify data files in FITS format. XSELECT is a command-line interface to the FTOOLS, for X-ray astrophysical analysis. The software is distributed by the *ASCA* Guest Observer Facility.

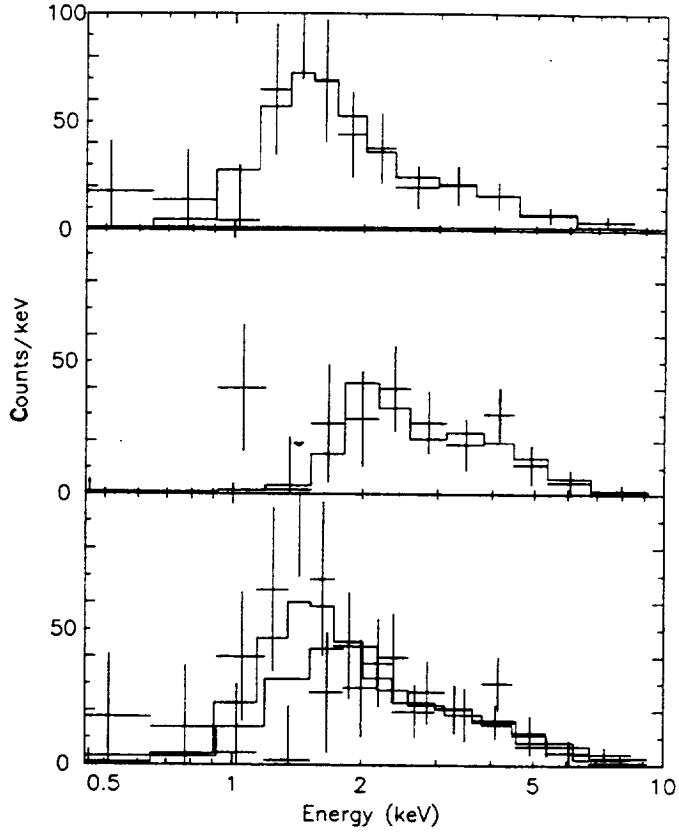

FIG. 2.—*ASCA* spectral data (*crosses*) with best-fit power law with fixed Galactic and intrinsic absorption models. *Top*: SIS; *middle*: GIS; *bottom*: both SIS and GIS.

The SIS and GIS spectra extracted in this way were then analyzed using XSPEC. The 1995 March release of the response matrices was used for the GIS data, and the 1994 November release for the SIS data. A power-law spectrum with fixed Galactic absorption (4.8×10^{20} atoms cm^{-2}; Stark

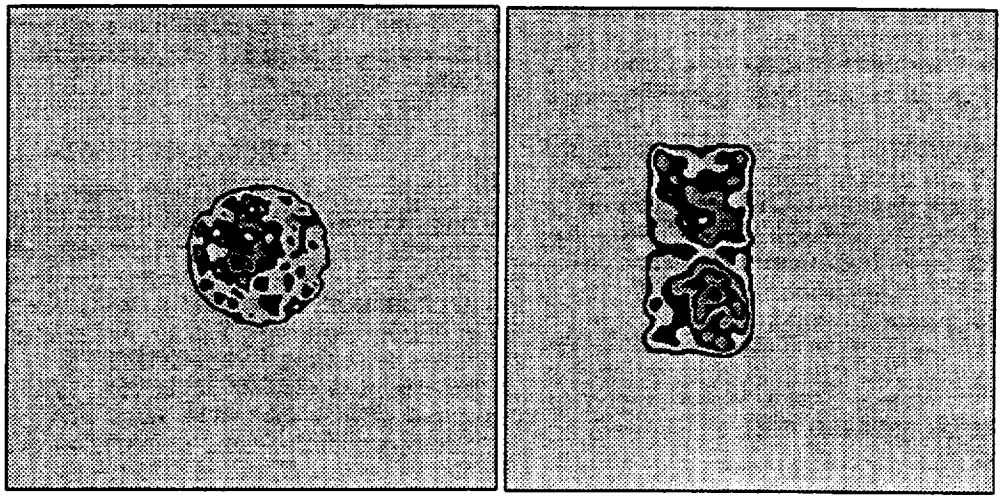

FIG. 1.—*ASCA* GIS3 (*left*) and SIS0 (*right*) gray-scale images around PHL 5200. North is 66°.7 clockwise from the top. The GIS field of view is 50′ in diameter, and each SIS chip is 11′.1 on a side (*ASCA* Technical Description 1993).

TABLE 2

SPECTRAL FITS TO *ASCA* DATA OF PHL 5200

Model	α_E	N_H (free)[a]	Normalization[b]	χ^2(dof)[c]
SIS				
Power law:				
+ N_H	$0.9^{+1.3}_{-1.0}$	$0.9^{+1.2}_{-0.8}$	$1.3^{+4.8}_{-0.3}$	5.2 (12)
+ N_H(Galactic) fixed	$-0.1^{+0.4}_{-0.4}$	...	$0.3^{+0.1}_{-0.2}$	8.4 (13)
+ $N_H(z = 1.98)$	$0.8^{+1.1}_{-0.9}$	$14.0^{+19.7}_{-12.4}$	$1.2^{+3.4}_{-0.4}$	4.8 (12)
GIS				
Power law:				
+ N_H	$2.0^{+3.1}_{-1.8}$	$4.5^{+0.0}_{-3.8}$	$9.6^{+875}_{-0.5}$	5.4 (9)
+ N_H(Galactic) fixed	$-0.1^{+0.5}_{-0.6}$	...	$0.3^{+0.2}_{-0.1}$	9.8 (10)
+ $N_H(z = 1.98)$	$2.8^{+6.2}_{-2.6}$	130^{+0}_{-118}	$47^{+170}_{-0.5}$	5.7 (9)
SIS + GIS				
Power law:				
+ N_H	$0.6^{+0.0}_{-0.7}$	$0.9^{+1.4}_{-0.7}$	$1.0^{+2.9}_{-0.4}$	14.1 (24)
+ N_H(Galactic) fixed	$-0.1^{+0.3}_{-0.3}$	...	$0.3^{+0.1}_{-0.2}$	18.4 (25)
+ $N_H(z = 1.98)$	$0.6^{+0.9}_{-0.6}$	$13.1^{+23.2}_{-11.1}$	$0.9^{+3.0}_{-0.4}$	14.2 (24)

[a] Times 10^{22} cm^{-2}.
[b] In units of 10^{-4} photons keV^{-1} cm^{-2} s^{-1} at 1 keV.
[c] Degrees of freedom in parentheses.

et al. 1992) provides an acceptable fit to the SIS0 data (Table 2). However, if absorption is allowed to be a free parameter, then the fit is improved with greater than 98% confidence (F-test; Table 2). The fitted value [$N_H(z = 0) = 9 \times 10^{21}$ atoms cm^{-2}; solar abundance] is much larger than the Galactic column density toward PHL 5200, indicating excess absorption along the line of sight. This is also much larger than the uncertainties in the SIS low-energy response, which may overestimate the column density by up to 2×10^{20} cm^{-2} (C. S. R. Day, Calibration Uncertainties [1995], *ASCA* GOF WWW page [URL: http://heasarc.gsfc.nasa.gov/docs/asca/cal_probs.html]). We then fitted a power-law spectrum with Galactic column and an additional column of absorber allowing its redshift to be free. We found no preferred redshift for the additional absorber. Fixing the absorber at the source gives a column density of $1.4^{+2.0}_{-1.2} \times 10^{23}$ cm^{-2} (90% confidence for one parameter; solar abundance). The power-law energy index is $\alpha_E = 0.8^{+1.1}_{-0.9}$.

For the GIS data, a similar fit of a power-law spectrum with fixed Galactic and additional $z = 1.98$ absorption is acceptable but does not constrain the parameters well because the data have large errors (Table 2).

A combined SIS and GIS analysis does constrain the parameters of the model slightly better (Fig. 3; Table 2). The column density at the source is $1.3^{+2.3}_{-1.1} \times 10^{23}$ cm^{-2}, and $\alpha_E = 0.6^{+0.9}_{-0.6}$. This excess absorption, above Galactic N_H, is required at 99% confidence (F-test).

The 2–10 keV (observed frame) flux is $2.9^{+13.9}_{-1.3} \times 10^{-13}$ ergs s^{-1} cm^{-2} (corrected for best-fit absorption), and a 2–10 keV (rest frame) luminosity is 9.3×10^{45} ergs s^{-1} ($H_0 = 50, q_0 = 0$). The flux in the *EXOSAT* ME band (2–6 keV observed) is $2^{+6}_{-1} \times 10^{-13}$ ergs s^{-1} cm^{-2}. This is smaller than the *EXOSAT* flux ($\sim 2 \times 10^{-12}$ ergs s^{-1} cm^{-2}; Singh et al. 1987) by at least a factor of 2.5. The optical continuum of PHL 5200 does not vary by such a large amount (Barbieri, Romano, & Zambon 1978). It is possible that it is variable absorption rather than intrinsic source variability that might be responsible for the difference in the *ASCA* and *EXOSAT* ME fluxes. The *ASCA* flux is consistent with the upper limits observed by the *Einstein* IPC (less than 4.5×10^{-13} ergs s^{-1} cm^{-2}) and the *EXOSAT* CMA (less than 5×10^{-13} ergs s^{-1} cm^{-2}).

The *ASCA*-derived monochromatic luminosity at 2 keV

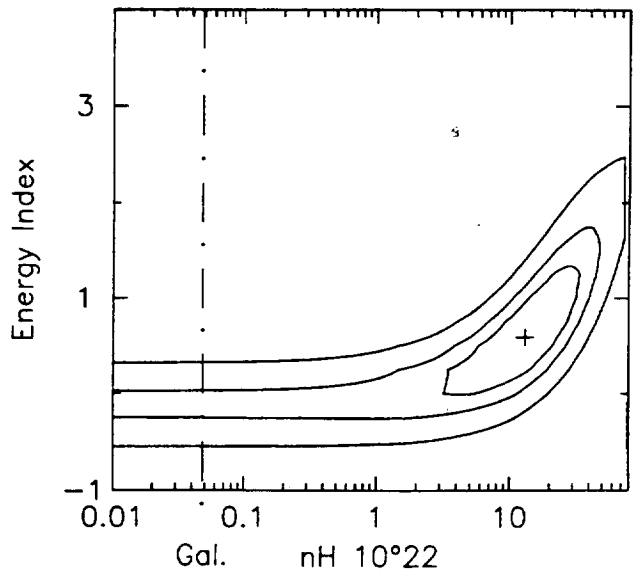

FIG. 3.—Confidence contours for the combined SIS and GIS spectrum. Contours of 68%, 90%, and 99% confidence regions are shown. The Galactic column density is shown as a dot-dashed line.

(rest frame) is 1.3×10^{28} ergs s^{-1} Hz^{-1}, and at 2500 Å (rest frame) it is 1.2×10^{32} ergs s^{-1} Hz^{-1} (Zamorani et al. 1981), giving $\alpha_{ox} = 1.5$.

An Fe K absorption edge is not detected ($\tau < 0.9$; 90% confidence for one interesting parameter). The opacity of an Fe edge corresponding to $N_H = 10^{23}$ cm^{-2} is $\tau = 0.1 f_{ion}$, where f_{ion} is the ionization fraction of iron in hydrogen-like state. Our data are not sensitive enough to detect such an edge.

The Fe K emission line (Ross & Fabian 1993) is also not detected (see Fig. 2). We place a 0.5 keV upper limit (90% confidence for one interesting parameter) to the rest-frame equivalent width of a narrow ($\sigma < 10$ eV) line between 2.1 and 2.4 keV (6.3–7.1 keV rest frame). This can be used to place an upper limit on the covering factor of the absorber. If the absorber is a uniform spherical shell surrounding the X-ray continuum source, then the Fe Kα line flux through recombination after photoionization of helium-like iron is given by $I_{line} = [N_H A(\mathrm{Fe})/10^{19.8}](\Omega/4\pi) I_{abs} \eta$ (Basko 1980), where η is the fluorescent yield, the efficiency with which the flux above 7.1 keV (I_{abs}) is reemitted as an Fe K line. Assuming solar abundance of iron [$A(\mathrm{Fe}) = 3.3 \times 10^{-5}$; Grevesse & Andres 1989] and $\eta = 0.5$ (Krolik & Kallman, 1987), we estimate the covering factor of the line emitting region, $\Omega/4\pi < 4 f_{ion}^{-1}$, which is not an interesting limit. If, however, the heavy-element abundance is 10 times solar (Hamann & Ferland 1993), then $\Omega/4\pi < 0.4 f_{ion}^{-1}$, consistent with Hamann et al. (1993).

3. DISCUSSION

The *ASCA* spectrum of PHL 5200 shows excess absorption at 99% confidence. A column density of $(0.2\text{–}4) \times 10^{23} (Z_\odot/Z)$ cm^{-2} is obtained if the absorber is at the source. A power law was a good fit to the data with the spectral slope ($\alpha_E = 0.6^{+0.9}_{-0.6}$) in the normal range (Wilkes et al. 1994). The PHL 5200 value of $\alpha_{ox} = 1.5$ is also normal for a radio-quiet quasar (Wilkes et al. 1994).

The inferred absorbing column density for PHL 5200 is 2–3 orders of magnitude larger than the earlier estimates of column density in BALQSOs (Hamann et al. 1993; Turnshek 1984). This implies that the BAL clouds may be more highly ionized ($N_{H\,I}/N_H \sim 10^{-8}$) than previously thought ($N_{H\,I}/N_H \sim 10^{-5}$; Hamann et al. 1993), as was true with narrow associated absorbers (Mathur et al. 1994, 1995). The estimates from the saturated UV lines appear to have been misleading. Recent models of BALQSOs (Murray et al. 1995), however, do consider column densities as large as we find in PHL 5200. If, on the other hand, the abundances are 100–1000 times solar, then the hydrogen column density would be smaller ($N_H \sim 10^{20}$ cm^{-2}). However, the ionization state would still be high, since the comparison is between metal line absorption in the UV and absorption in X-rays. The column density in PHL 5200 is also about an order of magnitude larger than other, narrow, associated absorption systems (Fiore et al. 1993; Turner et al. 1994). In this respect, as in velocity width, the BALQSOs may be extreme examples of other associated absorbers.

This is consistent with our earlier conjecture that all associated absorbers may form a continuum of properties with column density, outflow velocity, and the distance from the central continuum (Mathur et al. 1994). Are BALQSOs also similar to these in being "XUV absorbers," i.e., are the broad absorption lines observed in the UV caused by the same matter producing X-ray absorption? This can be investigated by combined analysis of X-ray and UV spectra (Mathur et al. 1994, 1995) of PHL 5200 but is beyond the scope of this paper. If they are indeed the same, it would allow us to further constrain the physical properties of the absorber and so of the outflowing circumnuclear matter (Mathur et al. 1995).

The present study implies that BALQSOs are not intrinsically X-ray quiet; it is the extreme absorption that makes them appear faint to low-energy experiments. Since the absorption is significant only in soft X-rays, hard X-ray observations, above a few keV, would reveal their presence as X-ray sources. This can be done with missions like *ASCA*, *XTE*, *SAX*, and *AXAF*. We have been awarded *XTE* time to observe BALQSOs with this aim.

This research has made use of the NASA/IPAC Extragalactic Database (NED), which is operated by the Jet Propulsion Laboratory, Caltech, under contract with the National Aeronautics and Space Administration. This work was supported by NASA grants NAGW-2201 (LTSA), NAG5-2563 (ASCA), NAGW-4490 (LTSA), and NASA contract NAS8-39073 (ASC).

REFERENCES

Barbieri, C., Romano, G., & Zambon, M. 1978, A&AS, 31, 401
Basko, M. M. 1980, A&A, 87, 330
Burbidge, E. M. 1968, ApJ, 152, 111
Fiore, F., Elvis, M., Mathur, S., & Wilkes, B. 1993, ApJ, 415, 129
Green, P. J., et al. 1995, ApJ, 450, 51
Grevesse, N., & Andres, E. 1989, in AIP Conf. Proc. 183, Cosmic Abundances of Matter, ed. C. J. Waddington (New York: AIP), 1
Hamann, F., & Ferland, G. 1993, ApJ, 418, 11
Hamann, F., Korista, K., & Morris, S. L. 1993, ApJ, 415, 541
Kopko, M., Turnshek, D. A., & Espey, B. 1993, in IAU Symp. 159, Quasars across the Electromagnetic Spectrum ed. T. J.-L. Courvoisier & A. Blencha (Dordrecht: Kluwer), 450
Krolik, J. H., & Kallman, T. R. 1987, ApJ, 320, L5
Lanzetta, K. M., Wolfe, A. M., Turnshek, D. A., Lu, L., McMahon, R. G., & Hazard, C. 1991, ApJS, 77, 1
Loewenstein, T., & Isobe, T. 1992, translation of *ASCA* Interim Rep., ISAS
Mathur, S. 1994, ApJ, 431, L75
Mathur, S., Elvis, M., & Wilkes, B. 1995, ApJ, 452, 230
Mathur, S., Wilkes, B., Elvis, M., & Fiore, F. 1994, ApJ, 434, 493
Murray, N., Chiang, J., Grossman, S. A., & Voit, G. M. 1995, ApJ, 451, 498
Ohashi, T., et al. 1991, Proc. SPIE, 1549, 9
Ross, R. R., & Fabian, A. C. 1989, MNRAS, 261, 74
Schneider, D. P., et al. 1992, PASP, 104, 678
Singh, K. P., Westergaard, N. J., & Schnopper, H. W. 1987, A&A, 172, L11
Stark, A. A., Gammie, C. F., Wilson, R. W., Bally, J., Linke, R., Heiles, C., & Hurwitz, M. 1992, ApJS, 79, 77
Stocke, J. T., Morris, S. L., Weymann, R. J., & Foltz, C. B. 1992, ApJ, 396, 487
Tanaka, Y., Holt, S. S., & Inoue, H. 1994, PASJ, 46, L37
Turner, T. J., Nandra, K., George, I. M., Fabian, A., & Pounds, K. A. 1994, ApJ, 419, 127
Turnshek, D. A. 1984, ApJ, 280, 51
———. 1988, in QSO Absorption Lines: Probing the Universe, ed. J. C. Blades, D. Turnshek, & C. Norman (Cambridge: Cambridge Univ. Press), 17
Ulrich, M. H. 1988, MNRAS, 230, 121
Weymann, R., Morris, S. L., Foltz, C. B., & Hewett, P. C. 1991, ApJ, 373, 23
Wilkes, B. J., Tananbaum, H., Worrall, D. M., Avni, Y., Oey, M. S., & Flanagan, J. 1994, ApJS, 92, 53
Zamorani, G., et al. 1981, ApJ, 245, 357

ASCA and *ROSAT* X-ray Spectra of High-Redshift Radio-Loud Quasars

M. Cappi[1,†], M. Matsuoka[1]; A. Comastri[2], W. Brinkmann[3],
M. Elvis [4], G.G.C. Palumbo[5,6] and C. Vignali[5]

[1] *The Institute of Physical and Chemical Research (RIKEN), 2-1, Hirosawa, Wako, Saitama 351-01, Japan*

[2] *Osservatorio Astronomico di Bologna, Via Zamboni 33, I-40126 Bologna, Italy*

[3] *Max-Planck-Institut für Extraterrestrische Physik, D-85748 Garching bei München, FRG*

[4] *Harvard-Smithsonian Center for Astrophysics, 60 Garden Street, Cambridge, Massachussets 02138, USA*

[5] *Dipartimento di Astronomia, Università di Bologna, Via Zamboni 33, I-40126 Bologna, Italy*

[6] *Istituto per le Tecnologie e Studio Radiazioni Extraterrestri, ITeSRE/CNR, Via Gobetti 101, I-40126 Bologna, Italy*

† *Present address: Istituto per le Tecnologie e Studio Radiazioni Extraterrestri, ITeSRE/CNR, Via Gobetti 101, I-40126 Bologna, Italy*

ABSTRACT

Results are presented on the X-ray properties of 9 high-redshift ($1.2 < z < 3.4$) radio-loud quasars (RLQs) observed by *ASCA* (10 observations) and *ROSAT* (11 observations, for a subset of 6 quasars). New *ASCA* observations of S5 0014+81 ($z = 3.38$) and S5 0836+71 ($z = 2.17$) and *ROSAT* observations of PKS 2126-158 for which results were never presented elsewhere, are included.

A simple model consisting of a power law plus cold, uniform absorption gives acceptable fits to the spectra of all sources. The *ASCA* spectra of the 6 brightest objects show evidence for absorption in excess of the Galactic value at a $\gg 99\%$ confidence level. Comparison with the *ROSAT* data suggests that absorption has significantly varied ($\Delta N_{\rm H} \sim 8 \times 10^{20}$ cm^{-2}) in the case of S5 0836+71, on a time-scale of ~ 0.8 yr in the quasar frame. For the remaining 5 sources for which *ROSAT* spectra were available, the two instruments gave consistent results and the data were combined yielding unprecedent spectral coverage (typically $\sim$ 0.4-40 keV in the quasar frame) for high-z quasars. This allows to put severe limits on several different descriptions of the continuum (e.g. broken power law, bremsstrahlung, reflection component). No Fe Kα emission line is detected in any of the *ASCA* spectra. An absorption edge consistent with Fe Kα at the quasar redshift is marginally detected in S5 0014+81. Possible origins for the observed low energy absorption are discussed. In particular, contributions from the molecular clouds and dust present in our Galaxy (usually disregarded) are carefully considered. In the light of the new results for S5 0836+71 and S5 0014+81, absorption intrinsic to the quasars is considered and discussed.

The average slope obtained from the 8 *ASCA* spectra in the observed $\sim$ 0.5–10 keV energy band is $< \Gamma_{0.5-10{\rm keV}} > \simeq 1.61 \pm 0.04$, with a dispersion $\sigma_{0.5-10{\rm keV}} \simeq 0.10 \pm 0.03$. The average photon index in the observed 2–10 keV band, where the effect of absorption is negligible, is $< \Gamma_{2-10{\rm keV}} > \simeq 1.53 \pm 0.05$, with a dispersion $\sigma_{2-10{\rm keV}} \lesssim 0.12$. Furthermore, the implications of the present results on the calculations of the contribution of quasars to the cosmic X- and γ-ray backgrounds (XRB and GRB) are briefly discussed.

Subject headings: galaxies: active — quasars: general — X-rays: galaxies

1. Introduction

Quasars are the most powerful objects in the whole Universe. This is especially true in the X-ray band, where luminosities can reach $\sim 10^{47-48}$ erg s^{-1}. However how quasars produce such a large amount of energy remains a challenging astrophysical problem. Certainly, because of their extreme conditions, quasars provide a powerful test for models of emission mechanisms of active galactic nuclei (AGNs) (Rees 1984). Quasars show strong continuum emission over the entire electromagnetic spectrum, from radio through the X- and even γ-ray region (Sanders et al. 1989, Elvis et al. 1994a, Thompson et al. 1995). Optically selected samples of quasars indicate that $\sim$ 90% of them are radio quiet (RQQs) and $\sim$ 10% are radio loud (RLQs).

X-ray quasar spectral observations are crucial for two main reasons: X-rays carry a large amount of the total quasar luminosity. Secondly, as demonstrated by observations of rapid X-ray variability, X-rays originate from the innermost regions of the quasar (Mushotzky, Done & Pounds 1993). Most X-ray spectral observations have included mainly low redshift ($z < 1$) quasars; the poor energy resolution generally limited the analysis to a simple parameterization of the spectrum with a single power law. In the $\sim$ 0.1–4 keV energy range, previous *Einstein* IPC and *ROSAT* PSPC observations have shown that RLQs have significantly flatter X-ray spectra than RQQs (Wilkes & Elvis 1987, Brunner et al. 1992) and that, for a given optical luminosity, RLQs are on average $\sim$ 3 times brighter in X-rays than RQQs (Zamorani et al. 1981). Studies at higher energies ($\sim$ 2–10 keV) with *EXOSAT* and *Ginga* have confirmed the dichotomy, with a clear correlation between spectral index and radio-loudness (Williams et al. 1992, Lawson et al. 1992). Whether differences in the observed X-ray properties should be attributed either to intrinsically different properties of the sources or inclination effects and/or host galaxy properties is not yet well understood. Also selection effects and/or complex spectral structures (e.g. soft-excess emission, ionized absorption) may complicate the correct interpretation of the data (Halpern 1984, Comastri et al. 1992, Fiore et al. 1993).

At high redshifts ($\gtrsim 1$), spectral information is almost absent for RQQs, and scarce for RLQs, since soft X-ray observations (mainly from the *ROSAT* PSPC) have allowed only a poor determination of the spectral slopes for only a small number of objects, mostly RLQs (Bechtold et al. 1994, Elvis et al. 1994b, hereafter E94). It is not yet clear whether quasars do exhibit spectral evolution. This is a fundamental question which has a direct impact on quasar formation models. A remarkable result has been the discovery made with the PSPC that at least some of the high-z RLQs have low energy cut-offs possibly due to absorption along the line of sight (E94). Preliminary results of *ASCA* observations of high-z RLQs have indeed already confirmed the low energy cut-off in two of them (Serlemitsos et al. 1994) and discovered a third probable case (Siebert et al. 1996, hereafter S96). Comparison with two high S/N spectra of two RQQs at $z \sim 1$ (Nandra et al. 1995) indicates that RQQs are steeper than RLQ even at $z \gtrsim 1$. However, the number of quasars observed so far is too small to draw any reliable conclusion.

This paper presents a comprehensive and uniform study of *ASCA* observations of a sample of 9 RLQs with $1.2 < z < 3.4$. Whenever possible, the *ASCA* results are compared and combined to *ROSAT* spectra extracted from the public archive. Extensive search for Fe K emission lines, high-energy excesses ("hard tails") and alternative models are presented. The possible origin of the apparently common excess absorption found in the data is discussed in the light of two newly discovered RLQs with such feature. Finally, the impact of these new measurements on the cosmic high energy background radiation is briefly discussed.

In the following, $H_0 = 50$ km s^{-1} Mpc^{-1} and q_0=0 are assumed throughout.

2. Observations and Data Analysis

2.1. The Sample

The quasar sample consists of all objects (9) either from PI or archival *ASCA* observations available before 1996, January 1st. The purpose was to analyze data of a reasonably large number of quasars to be able to address for the first time statistically the X-ray properties of the class.

A total of 10 *ASCA* pointed observations were collected, with S5 0014+81 observed twice. For five quasars, 11 *ROSAT* PSPC observations were retrieved from the archive and the source spectra re-analyzed to ensure a uniform and consistent analysis within the sample. A considerable part of our analysis reproduces in part previous work on individual sources (see §4). The present analysis, however, differs from single object studies as: a) it provides a uniform analysis of the quasar sample, b) it makes use of the most recent calibrations (particularly important for those observations performed during the Performance and Verification phase of *ASCA*) and c) it compares on a uniform basis *ASCA* and *ROSAT* spectral results. It is worth pointing out that *ASCA* results on S5 0014+81 (z=3.38) and S5 0836+71 (z=2.17) are new. The relevant data for the whole sample are given in Table 1.

2.2. *ROSAT* Data Reduction

A sub-sample of six of the 9 quasars were observed on-axis with the Position Sensitive Proportional Counter (PSPC) (Pfefferman et al. 1987) on board

the *ROSAT* Observatory (Trümper 1983) between 1991 and 1993. The relevant data for the observations are listed in Table 2. As indicated in the Table, two new PSPC observations of PKS 2126-158 are presented, which almost double the total number of counts available for that source. The PSPC has an energy bandpass in the range 0.1–2.4 keV with an energy resolution of $\Delta E/E \sim 0.5$ keV at 1 keV. Source spectra were extracted from circles of $\sim$ 90"–200" centered on the sources, and background spectra were taken from annuli centered on the sources or from circular regions uncontaminated by nearby sources. Source and background counts were corrected for telescope vignetting. Data preparation and analysis were performed using the JAN95 version of the EXSAS/MIDAS software package (Zimmerman et al. 1993). Spectral analysis was performed using the version 8.50 of the XSPEC program (Arnaud, Haberl & Tennant 1991).

2.3. *ASCA* Data Reduction

ASCA has two gas imaging spectrometers (GIS) and two solid-state imaging spectrometers (SIS) (Tanaka, Inoue & Holt 1994). The energy resolution of the GIS and SIS are $\Delta E/E \sim 0.15$ keV and ~ 0.05 keV at 1 keV, respectively, which is about 3 and 10 times better than the *ROSAT* PSPC. The SIS was operated in 1-CCD, 2-CCD or 4-CCD modes, depending on the observation (see Table 3). Only chip n.1 of SIS0 and chip n.3 of SIS1 were used in the analysis of the SIS data, except for the AO1 observation of S5 0014+81 where also chip n.2 of SIS1 was used because the source photons were spread equally over the two detectors. Following a software-related problem on board *ASCA*, the data collected from the GIS3 during the observation of PKS 0537-286 were damaged. They could not be recovered as described in the *ASCA* ABC guide and therefore were excluded from the analysis. All observations were performed in FAINT mode and were corrected for dark frame error (DFE) and echo uncertainties (Otani & Dotani, 1994). The data were selected according to standard (rather conservative) criteria, i.e., when the angle between the target and the Earth's limb was $> 5°$ (SIS and GIS), when the geo-magnetic rigidity was > 7 GeV/c (GIS) and > 8 GeV/c (SIS) and when the angle between the target and the day-night terminator was $> 25°$ (SIS). Rise-time rejection was applied to the GIS data, and hot and flickering pixels were removed from the SIS data. Telemetry drop-outs and spikes were excluded from the light curves for each instrument.

Source counts were extracted from circles centered on the sources of 6′ for the GIS and 3′ for the SIS. For the SIS instruments, the background spectra were obtained from the edges of the same CCD chip. The use of SIS blank sky files for the background yielded spectral results within the errors reported in the following analysis. For the GIS instruments, we found that the two standard background substraction methods (backgrounds extracted from the blank sky files or locally) gave systematically different results for the weakest sources. Therefore, a non-standard background extracted from the blank sky standard files was adopted. Detailed explanation and justification for this choice is given in the Appendix A.

The relevant data for the *ASCA* observations are given in Table 3. Data preparation and spectral analysis were performed using version 1.0h of the XSELECT package and version 8.50 of the XSPEC program (Arnaud et al. 1991).

3. Results

3.1. *ROSAT* Temporal and Spectral Analysis

The data were first binned in 400 s time intervals, as suggested by the wobble period of the telescope, and light curves were plotted to evidence variability. However, no significant variation was detected. Source spectra were thus accumulated for each observation, and binned with a signal to noise ratio from 4 to 13, depending on the source statistics. Three quasars (PKS 0438-436, S5 0836+71 and PKS 2126-158) had multiple observations. Comparisons between different observations indicate a clear flux variation for S5 0836+71, and possibly for the other two quasars. These are discussed in detail in §4 where results for individual sources are presented. After preliminary analysis, no significant spectral variability was detected between the multiple observations. These were, therefore, fitted simultaneously, tying together the fit parameters, but with the normalizations free to vary.

Fits were performed using a single absorbed power law model with absorption cross-sections and abundances from Morrison & McCammon (1983). The resulting spectral photon indices Γ, column densities $N_{\rm H}$ and normalizations are given in Table 4. The two-dimensional χ^2 contour plots in the parameter space $N_{\rm H}$–Γ are shown in Fig. 1, together with the *ASCA* contours (see §3.2). The present re-analysis yielded results consistent with previous measurements (see references in Table 2). It is worth pointing out that the absorption in excess of the Galactic value previously reported for PKS 0438-436 and PKS 2126-158 (Wilkes et al. 1992, E94) is confirmed by the present analysis (see Fig. 1 or Table 4), which makes use of two new PSPC observations of PKS 2126-158 almost doubling the total counts from that source. The weighted mean photon index for the PSPC sample is $< \Gamma_{0.1-2.4{\rm keV}} > \simeq 1.53 \pm 0.06$.

More complex models were not attempted since a) the main purpose of the present analysis of *ROSAT* observations is to compare and, whenever possible, combine these data with the *ASCA* data and b) in all cases, a single absorbed power law model provides an accept-

able description of the spectra. More complex models might, however, be found in the references given in Table 2.

3.2. *ASCA* Temporal and Spectral Analysis

Source plus background light-curves were accumulated for each source, and none of these indicated significant variability. This is not surprising given the large statistical scatter of the data due to the low counting rates. GIS and SIS spectra were binned with more than 20 counts/bin between $\sim$ 0.7–10 keV and $\sim$ 0.5–10 keV, respectively. The matrices used were the gis[23]v4-0.rmf released in June 1995 for the GIS and the "rsp1.1alphaPI" matrices released in October 1994 for the SIS. Since the spectral parameters obtained by separately fitting the four detectors were all consistent at a $\sim$ 90% confidence level, the data were fitted simultaneously from all four instruments with the same model, tying the fit parameters together but allowing the relative normalizations of the four datasets to vary.

The spectra were first fitted using a single absorbed power law model with all parameters free to vary. The resulting best-fit parameters are given in Table 5, together with the absorbed 2–10 keV flux and intrinsic 2–10 keV luminosity derived from the fits. In each case, a single absorbed power law model provides an acceptable description of the spectra. The two-dimensional χ^2 contour plots in the parameter space $N_{\rm H}$–Γ are shown in Fig. 1, together with the *ROSAT* contours. Contours representing the 68%, 90% and 99% confidence limits for two interesting parameters are indicated for the simultaneous fit of the GIS and SIS data. The 90% confidence contours obtained from separately fitting GIS and SIS are indicated as well. They clearly show that the spectral parameters obtained from the GIS always agree with the SIS results at least at a 90% confidence level. The elongated shape of the GIS contours in the direction of low column densities is a consequence of the reduction of the GIS effective area at low (E $\lesssim$ 0.8 keV) energies, where the effect of the absorption is highest; to be compared with the SIS detectors sensitive down to E $\sim$ 0.4–0.5 keV. The much smaller phase space occupied by the *ASCA* χ^2 contours compared with *ROSAT*, in particular for S5 0014+81 and NRAO 140, indicate the higher capabilities of *ASCA* to constrain both the photon index (because of the larger energy band) and column density (because of the higher statistics).

The contours also clearly show that at least 5 quasars: S5 0014+81, PKS 0438-436, S5 0836+71, PKS 2126-158 and PKS 2149-306, have $N_{\rm H}$ values larger than the Galactic one, at a more than 99% confidence level. For the three Parkes sources, the present results confirm previous findings by Serlemitsos et al. (1994) and S96 obtained with the same *ASCA* data. The most important results are instead for S5 0014+81 and S5 0836+71 for which excess absorption is detected for the first time, at a high (> 99.99%) confidence level (Fig. 1). The previous analysis of the *ASCA* observation of S5 0014+81 by Elvis et al. (1994c) didn't show any excess absorption as only the GIS data had been analyzed, thus sensitivity at low energies to detect the excess absorption was lost. A striking result from the present analysis comes from comparing the *ROSAT* and *ASCA* contours for S5 0836+71 (Comastri, Cappi & Matsuoka 1996) **which indicates** a large variation in the absorption column density of $\sim 8 \times 10^{20}$ cm^{-2} (see §4.6 for details).

It should be noted, however, that although the χ^2 contour plots of Fig. 1 show that the *ASCA* and *ROSAT* parameters are always consistent within their 90% confidence levels (except for S5 0836+71), the same contours also indicate that the best-fit column densities obtained with *ASCA* are systematically larger than the *ROSAT* values. **There are several possibilities to explain this apparent contradiction: (1) all quasars experienced a real increase in the absorption column densities (between $\sim$ 6–15 $\times$ 10^{20} cm^{-2}; (2) all the excess absorption is due to SIS calibration uncertainties at low energies; (3) the absorption measured by *ASCA* (corrected for the calibration uncertainties estimated below) is real and the difference between the *ASCA* and *ROSAT* results is due to a) the increased statistic obtained with *ASCA* or b) the fact that the absorption is more complex than the adopted one (i.e. a warm absorber). Absorption variability (1) can be disregarded as there is no reason to expect such increase in all quasars. In order to quantify any systematic instrumental effect (2) of the SIS at low energies, a series of tests described in detail in Appendix B have been applied.** Results from this study indicate that part ($\sim$ 2–3 $\times$ 10^{20} cm^{-2}) of the excess absorption column density measured in the quasars can indeed be attributed to remaining SIS calibration uncertainties. However it is very unlikely that the effect is all instrumental since even after considering a conservative systematic error of $\sim$ 3–4 $\times$ 10^{20} cm^{-2} (estimated by us in the Appendix B and, independently, by Hayashida et al. 1995), the measured column densities are still significantly higher than the Galactic values. Also in the light of the fairly good agreement between the *ROSAT* and *ASCA* results, in particular for PKS 0438-436 and PKS 2126-158 (see Fig. 1), we are inclined to interpret these excess absorptions as real. **Possibilities (3a) and (3b), therefore, are the most plausible and will be further considered below (see §3.3.2).**

The weighted mean photon index obtained for the whole sample in the observed $\sim$ 0.5–10 keV is $< \Gamma_{0.5-10{\rm keV}} > \simeq 1.59 \pm 0.01$ with a dispersion $\sigma_{0.5-10{\rm keV}} \simeq 0.10$ when $N_{\rm H}$ is left free to vary and 1.45 ± 0.01 with

a dispersion of 0.08 when N_H is fixed at the Galactic value. However, fits with the absorption fixed at the Galactic value (Table 5) are not acceptable for these quasars because clear depressions appear at low ($\lesssim$ 1 keV) energies in the residuals of SIS and, in some case, of GIS. The mean slope and dispersion have also been computed, jointly, using a maximum-likelihood technique (see Maccacaro et al. 1988) which has the advantage, over a simple algebraic mean, of weighting the individual photon indices according to their measured errors assuming a Gaussian intrinsic distribution of spectral indices. The results obtained in this way are $< \Gamma_{0.5-10keV} > \simeq 1.61 \pm 0.04$ and $\sigma_{0.5-10keV} = 0.10 \pm 0.03$, where the confidence intervals are the 68% level for two interesting parameters. Fitting the data only between 2–10 keV where the effect of the absorption is negligible gives $< \Gamma_{2-10keV} > \simeq 1.53 \pm 0.05$ and $\sigma_{2-10keV} \lesssim 0.12$.

The *ASCA* spectra were also investigated for the presence of Fe Kα emission lines. Given the high redshifts of the quasars, Fe Kα lines are expected at energies between $\sim$ 1.5 and 3 keV, where GIS and SIS effective areas and resolution are highest. No significant Fe Kα emission lines were detected, with upper limits for the equivalent width of a narrow Gaussian line at 6.4 keV ranging between 40 and 415 eV (quasar frame, Table 5). Very similar upper limits were obtained for a line emitted at 6.7 keV in the quasar frame. Next, spectra were searched for neutral Fe K edges at 7.1 keV (quasar frame) and, for ionized Fe K edges, at the mean energy of 7.8 keV observed in Seyfert 1 galaxies (Nandra & Pounds 1994). Whenever these spectral features were expected in the energy range of 1.8–2.4 keV, a conservative systematic error of 10 eV (for the lines) and $\Delta\tau = 0.05$ (for the edges) were added to take into account the uncertainties of the *ASCA* response at these energies (Table 5). No absorption edges were detected except for S5 0014+81. For this quasar, the inclusion of an absorption edge at E $\simeq 1.62 \pm 0.1$ keV (E $\simeq 7.1 \pm 0.4$ keV in the quasar frame) with depth $\tau \simeq 0.15^{+0.12}_{-0.11}$ corresponds to a $\Delta\chi^2 \simeq 9$ which is significant at more than 90% confidence. The detection is also supported by the fact that the edge seems to be present in both observations (October 93 and October 94), at 68% and 99% confidence level, respectively. The equivalent hydrogen column density derived from the edge is $\sim (4-39) \times 10^{23}$ cm^{-2} (assuming a Fe cosmic abundance relative to hydrogen of $\sim 3 \times 10^{-5}$) which is consistent with $\sim (4-7) \times 10^{23}$ cm^{-2} measured assuming an intrinsic origin for the absorber (Table 6). The predicted Fe Kα line equivalent width is in the range of $\sim$ 40–350 eV (Makishima 1986, Leahy & Creighton 1993) consistent with the computed upper limits.

3.3. *ROSAT* and *ASCA* Combined Temporal and Spectral Analysis

For five of the nine quasars: S5 0014+81, NRAO 140, PKS 0438-436, PKS 0537-286 and PKS 2126-158, the best-fit spectral parameters derived from *ROSAT* and *ASCA* data are consistent with each other at a 90% confidence level. Despite the fact that the *ASCA* spectra require systematically more absorption than the *ROSAT* spectra (see Appendix B), the 0.1–2 keV flux extrapolated from the *ASCA* spectra (Table 5) is in good (within $\sim$ 10%) agreement with the measured *ROSAT* flux (Table 4). Therefore, the data from the two instruments were combined to benefit of the higher sensitivity of the *ROSAT* PSPC at lower energies and of the *ASCA* instrument higher energy resolution and broad band. The unprecedented quality (for high-z quasars) of these combined spectra, covering typically an energy range of $\sim$ 0.4–40 keV in the quasar frame, provide an excellent opportunity to test the data against more complex emission models such as complex absorption, thermal emission and reflection models, as described in the following.

3.3.1. Single Power-Law Fits

Again, we first fitted the combined spectra with a single absorbed power law model, with absorption abundances and cross-sections from Morrison & Mc Cammon (1983). The results from these fits are given in Table 6. Spectra, residuals and contour plots are shown in Fig. 2. The weighted mean of the photon indices for the 5 quasars is $< \Gamma_{0.1-10keV} > \simeq 1.62 \pm 0.02$, with a dispersion $\sigma_{0.1-10keV} \simeq 0.11$. Note that, when compared with *ASCA* results alone (Table 5), the addition of *ROSAT* data for S5 0014+81 and NRAO 140 gives almost unchanged results. However, for the other three sources: PKS 0438-436, PKS 0537-286 and PKS 2126-158, there is indeed a significant improvement combining the data. Note that the column density for PKS 0537-286 turns out to be marginally (> 90%) higher than the Galactic value since statistical errors have been reduced, suggesting excess absorption in this source too. However, considering the *ASCA* SIS systematic uncertainties (Appendix B), conclusions on this issue are unwarranted.

The inclusion of an Fe K emission line or Fe K absorption edge in the model gave results almost identical to the one obtained in §3.2 and given in Table 5.

3.3.2. Absorption Fits

Given sufficient energy resolution, it should in principle be possible to constrain the redshift and metal abundances of a neutral absorber through direct spectral fitting. Though such measurements sound difficult with present generation X-ray telescopes, it might be worth trying them with the best available data.

As a first step, therefore, elemental abundances were fixed at the cosmic value, given by Morrison & Mc Cammon (1983), and spectral fittings with two separate absorbers, one at z=0 fixed at the Galactic value, and one at the quasar redshift with N_H free were repeated. The resulting parameters are given in Table 6. Accordingly, the column densities obtained for an absorber intrinsic to the quasar are larger, ranging between $\sim$ 1.7–55 $\times$ 10^{21} cm^{-2}. If the redshift of the absorber is left free to vary, no preferential solution is found for any of the quasars indicating that the present data do not allow to distinguish between a local absorber (at z=0) or any other absorber placed between us and the quasars. **If the abundances of the metals (C, N, O, Ne, Mg, Si, S, Ar, Ca, and Fe) were tight together and left free to vary (increasing by one the number of degrees of freedom), no constrain was obtained on the abundances. This indicates that the model was too complex for the present data and no information on the metal abundances of the absorber could be obtained.**

The spectra were then fitted again with a single absorbed power law model but this time the Morrison and McCammon cosmic abundances for the photo-electric absorption (placed at z=0) were replaced with more recent abundances values obtained by Anders & Grevesse (1989) and Feldman (1992). The two cases gave systematically lower absorption column densities by up to $\sim$ 12% and 10%, respectively. Since these differences were, in every case, within the reported statistical errors, they do not substantially modify the present conclusions. This systematic difference should, however, be kept in mind in particular for future, more sensitive, X-ray missions.

It should be pointed out, however, that the absorber could be ionized (Krolik & Kallman 1984) as is commonly observed in Seyfert 1 galaxies (e.g. Otani 1995). If present, a warm absorber should imprint two main characteristic features in the low energy spectrum: absorption edges at $\sim$ 0.7–1 keV (quasar frame) due to OVII and OVIII and extra emission below $\sim$ 0.7 keV due to the reduced warm absorber opacity at low energies. None of these features are observed in the present data. However, this is not surprising since, for a quasar at z = 2, the energy range for the edge features is redshifted to $\sim$ 0.2–0.4 keV which falls outside the *ASCA* energy range and the extra emission is expected below $\sim$ 0.2 keV where the PSPC response drops down rapidly. Moreover, since the present spectra indicate that the *ROSAT* spectra were typically less absorbed than the *ASCA* spectra (§3.2), this may be somehow the signature of a warm absorber. In order to test this hypothesis, a warm absorber model ("absori" in the XSPEC package) placed at the quasars' redshift has, therefore, been directly fitted to the data. Free parameters were the ionization parameter ($\xi = L/nR^2$ (ergs s^{-1} cm), where n is the warm gas density and R the distance of the absorber from the source), and the warm column density N_W (cm^{-2}); Magdziarz & Zdziarski 1995). A temperature of 3 $\times$ 10^4 K (Reynolds & Fabian 1995) and Fe cosmic abundances were assumed. Results are reported in Table 6. Though the fits are generally statistically worse than with a single absorbed power law model, the data accumulated to date do not rule out this model and are consistent with ionization parameters of the order of $\sim$ few tens up to few hundreds ergs s^{-1} cm with warm column densities ranging between $\sim$ 2–7 $\times$ 10^{22} cm−2.

3.3.3. Alternative continuum models

The possibility that other continuum models could be applied to the data was considered in the attempt to explain the low energy cut-off with Galactic absorption only and/or provide an alternative description of the higher energy power law spectrum.

A model consisting of a broken power law with the absorption column density fixed at the Galactic value was first applied in order to check whether a flat power law is able to describe the observed low energy cut-off. The spectral curvature may, indeed, be a property of the intrinsic emission of the quasars, as a break in the continuum is expected if the emission is due to the synchrotron mechanism where radiative losses are likely to steepen the spectra at higher energies. Similar arguments are often used to explain the convex shape of the X-ray spectra of BL Lac objects (e.g. Barr, Giommi & Maccagni 1988). The results of these fits are shown in Table 6. In order to obtain acceptable fits, the soft component is required to be very flat with typical values of the photon index < 1, while the photon index of the hard component is basically identical to the values found with a single power law model. In the four cases where the break energies are constrained, they are found to be in the $\sim$ 0.7–1.5 keV energy range in the observer frame. These fits are statistically acceptable and, in principle, very flat spectra could be explained, for example, in the framework of Inverse Compton models assuming a particular energy distribution of the electrons population (i.e. with a convex shape produced by the effect of radiative cooling at high energy and escape at low energies (Ghisellini, private communication)). This model therefore cannot be directly ruled out. However, considering that the broken power law model requires an extra free-parameter and that, statistically, it is never significantly better than the single absorbed power law model, using this model is unjustified with the present data.

The data were then fitted with a thermal bremsstrahlung model. With the absorption fixed at the Galactic value, this model is also not acceptable because there are significant and systematic deviations in the residuals at low (E $\lesssim$ 1 keV, observer frame) energies. **With free absorption, we find that the spectra can also be described by a very high temperature (kT $\sim$ 20–90 keV in the source frame) thermal model and an absorption slightly reduced (but still significantly (>99%) higher than the Galactic column) when compared to the single absorbed power law model (Table 6). The fits are, however, in all cases worse than with a single power law model. Note, moreover, that at these temperatures, a bremsstrahlung emission model is virtually indistinguishable from a flat power law in the *ASCA* energy range and as already noted by S96, these temperatures correspond to $\sim$ 10–15 keV in the observer frame, which is suspiciously similar to the *ASCA* higher energy limit. Since the temperature of bremsstrahlung emission is primarily determined by its high energy cut-off, only relatively poor constraints can be set with *ASCA* on this parameter (errors of $\sim$ 25–90%, see Table 6). As a result, the description given with the power law model is preferable, and the thermal model will not be considered any further.**

Previous *Ginga* results (Nandra & Pounds 1994) have shown that the canonical X-ray slope ($\Gamma \sim 1.7$) of Seyfert 1 galaxies can be interpreted as the sum of an intrinsic steep power law with $\Gamma_{2-20keV} \sim 1.8 - 2.1$ plus a reflection component (e.g. Lightman & White 1988). Prompted by these results and the fact that the present sample of quasars exhibit fairly flat ($\Gamma \sim 1.5 - 1.7$) spectra up to $\sim$ 30–40 keV (rest frame), we searched for evidence of high-energy flattening. A reflection component was included into the absorbed power law model leaving the absorption and photon index free to vary. **In its simplest form, this model (plrefl in XSPEC) adds only one free parameter: the relative normalization, R ($=A_{refl}/A_{pl}$), between the reflected component (A_{refl}) and the incident power law (A_{pl}). Present results give no evidence for a reflection component, with upper limits of R ranging from $\sim$ 0.3 to $\sim$ 0.7, at 90% confidence limit for two interesting parameters (Table 6). The lack of Fe K emission lines further supports this conclusion.**

????? Figure 5 shows a comparison of the distribution of the Fe K line equivalent widths (EW) obtained for a sample of Seyfert 1 galaxies (Nandra & Pounds 1994) and the upper limits obtained for the present sample. ?????

In order to test the consistency of the present results with what is commonly found in Seyfert 1 galaxies, we forced the intrinsic power law to be steep, with a photon index fixed at $\Gamma = 1.9$ and fitted the data again. As a result, the model spectra required a substantial amount of reflection, R $\sim$ 1.1 to 3.1, in order to explain the observed flat spectra. However, since all the fits became significantly worse ($\Delta\chi^2 \sim$ 10–20), the presence of such a reflection component can be ruled out on statistical basis.

4. Comments on Individual Objects

4.1. S5 0014+81

S5 0014+81 is the farthest and optically brightest quasar in this sample. It was observed in X-rays by *EXOSAT* in 1984 (Lawson et al. 1992), by the *ROSAT* PSPC in 1991 (E94, Bechtold et al. 1994) and by *ASCA* in 1993 and 1994. The GIS data obtained from the first of the two *ASCA* observations are discussed by Elvis et al. (1994c). Their results are in very good agreement with the present GIS results. The *ROSAT* image indicates that there are two X-ray sources within $\sim 6'$ of the quasar. One source at about 1.8′ from the quasar was excluded from the *ROSAT* analysis and was estimated to be negligible in the *ASCA* energy band. The other source, a $V = 8.8$ K0 star at $\sim 5'$ from the quasar was neglected for both instruments. The photon index and column density derived here (Table 5) are consistent with previous measurements. Considering the instrumental uncertainties and different instrumental band-passes, the *EXOSAT* and *ROSAT* PSPC spectra are consistent in both spectral index and flux to the *ASCA* results. However, it is the first time that the column density is clearly constrained at a value higher than the Galactic column at a high (>99.99%) significance level (Fig. 2). The absolute amount of excess absorption is $\sim 13.4 \times 10^{20}$ cm^{-2}. It should be noted that S5 0014+81 is well-known for its Lyman Limit absorbers which have been object of extensive studies (e.g. Steigman 1994 and references therein), but that no damped Lyα system is known along the line of sight to this quasar (Lanzetta, Wolfe & Turnshek 1995).

4.2. PKS 0332-403

This object was observed in the *ROSAT* All-Sky Survey (RASS) with a flux between 0.1–2.4 keV of $1.75 \pm 0.6 \times 10^{-12}$ erg cm^{-2} s^{-1} (Brinkmann, Siebert & Boller 1993). This is in reasonable agreement with the *ASCA* flux of $\sim 0.96 \pm 0.1 \times 10^{-12}$ erg cm^{-2} s^{-1} extrapolated between 0.1–2.4 keV and corrected for absorption. The *ASCA* observations were studied by S96, who derived spectral parameters consistent with our results.

4.3. NRAO 140

NRAO 140 has a long history of X-ray observations. Previous *HEAO-1*, *Einstein*, *EXOSAT* and *Ginga* observations have shown that its X-ray spectrum is well

described by a single absorbed power law with $\Gamma \sim 1.5$–1.8 (Marscher 1988, Ohashi et al. 1992). This source is known for showing a large and variable X-ray absorption column ($N_{\rm H} \sim 3$–20×10^{21} cm^{-2}) which has been interpreted as the passage of Galactic dense clouds across the line of sight (Bania, Marscher & Barvainis 1991). *ROSAT* and *ASCA* observations are given in Turner et al. (1995). Their combined fit yields $\Gamma \simeq 1.73 \pm 0.03$ and $N_{\rm H} \sim 3 \pm 2 \times 10^{21}$ cm^{-2} which is nearly identical to the present results (Table 6). The X-ray absorption column is significantly larger than the Galactic HI column density ($N_{\rm HI} \simeq 14.2 \times 10^{20}$ cm^{-2}; Elvis et al. 1989) derived from measurements at 21 cm. However, ^{12}CO emission measurement toward NRAO 140 implies a molecular hydrogen column density of ($N_{\rm H_2} \simeq 17 \times 10^{20}$ cm^{-2}) which, when added to the HI column density, is in excellent agreement with the observed X-ray column (Bania et al. 1991; Turner et al. 1995). These results confirm that the excess and variable absorption in NRAO 140 plausibly originates from Galactic molecular clouds passing accross the quasar line of sight. It should be noted, however, that these results are based on the assumption that the CO-to-H_2 conversion factor is $\sim 3 \times 10^{20}$ cm^{-2} K^{-1} km^{-1} s, as commonly found for clouds in the Galactic plane. But this value is rather uncertain in the case of high-latitude molecular clouds such as those toward NRAO 140. Assuming the much lower conversion factor of $\sim 0.5 \times 10^{20}$ cm^{-2} K^{-1} km^{-1} s obtained by de Vries, Heithausen & Thaddeus (1987) or Heithausen et al. (1993), the molecular hydrogen column density is reduced by a factor of ~ 6 and implies, again, excess absorption. It should also be noted that absorption intrinsic to the quasar is not ruled out by the current data.

4.4. PKS 0438-436

The *ROSAT* observations of this object were discussed in great detail by Wilkes et al. (1992) and E94 and its spectral energy distribution is shown in Bechtold et al. (1994). As E94 noted, the apparent flux decrease by $\sim 30\%$ between the two *ROSAT* observations (Table 4) can be explained if one takes into account the different wobble mode between the observations. Preliminary results of the *ASCA* observation are given in Serlemitsos et al. (1994) and are consistent with these presented here.

4.5. PKS 0537-286

The *ROSAT* and *ASCA* observations of PKS 0537-286 were previously discussed by Bühler et al. (1995) and S96, yielding results consistent with the present analysis. As shown in §3.3.1, combining the *ROSAT* and *ASCA* spectra, there is marginal evidence for excess absorption also in this quasar , **though, within the uncertainties in the low-energy response of the SIS. Note, however, that even after removing all the SIS data below 1.5 keV, the excess absorption remains statistically significant at > 90% confidence level.**

4.6. S5 0836+71

As Brunner et al. (1994) noted, S5 0836+71 underwent a flux decrease by a factor of ~ 2 between the two *ROSAT* observations (Table 4), with no evidence of spectral variation. The time scale of the variation corresponds to ~ 0.2 yr in the quasar frame. The present analysis shows that the *ASCA* flux is consistent with the *ROSAT* flux in the lower state. Compared with the *ROSAT* spectra, the *ASCA* results provide strong evidence for variable absorption ($\Delta N_{\rm H} \sim 8 \times 10^{20}$ cm^{-2}) in the direction of S5 0836+71 on a time-scale of less than 2.6 yr. Including in the model the Galactic absorption and assuming that the extra absorption is intrinsic to the quasar, the *ASCA* fits gives an intrinsic $N_{\rm H} \simeq 1.18^{+0.42}_{-0.37} \times 10^{22}$ cm^{-2}. The change in absorption corresponds then to a $\Delta N_{\rm H} \sim 1 \times 10^{22}$ cm^{-2} on a time-scale of $\lesssim 0.8$ yr in the quasar frame. It should be emphasized that fitting the *ASCA* spectra with a broken power law model absorbed by the Galactic column gives $\Gamma_{\rm soft} < 0.65$, $E_{\rm break}$ $0.96^{+0.09}_{-0.10}$ keV and $\Gamma_{\rm hard} \simeq 1.37^{+0.04}_{-0.03}$, with a fit formally acceptable ($\chi^2_{\rm red}$/dof $\simeq$ 0.87/502). However, as in the other cases where this model was applied (§3.3.3), this model requires the soft component to be extremely flat which is unphysical. It is interesting to note that S5 0836+71 has also been observed several times with EGRET in the high energy γ-ray band (Nolan et al. 1996). The reported spectrum is very steep ($\Gamma \simeq 2.5 \pm 0.5$) regardless of the (variable) γ-ray intensity.

4.7. PKS 1614+051

PKS 1614+051 was marginally detected with the *Einstein* IPC (Wilkes et al. 1994) and in the RASS (S96). The source is very faint also in the *ASCA* observation with a 2–10 keV flux of $\sim 2 \times 10^{-13}$ erg cm^{-2} s^{-1}.

4.8. PKS 2126-158

PKS 2126-158 was first detected in X-rays with the *Einstein* IPC (Zamorani et al. 1981). The *ROSAT* spectrum is discussed in E94 and the spectral energy distribution is given in Bechtold et al. (1994). Note that two additional *ROSAT* observations have been analyzed in the present work which almost doubled the total number of *ROSAT* counts. The *ASCA* observations were discussed by Serlemitsos et al. (1994), who tentatively constrained the redshift of the absorber at z<0.4. However, we cannot reproduce such contours, neither with nor without the addition of the *ROSAT* data. No redshift is preferred from our analysis. This

discrepancy might be attributed to the fact that Serlemitsos et al. use older response matrices obtained from the preliminary calibrations of the GIS and SIS instruments.

4.9. PKS 2149-306

RASS and *ASCA* observations of PKS 2149-307 were discussed in S96. The comparison of the spectra obtained from the two instruments indicates spectral variability in this source, most likely interpreted in terms of variable absorption (see Fig. 2 of S96). The column density found in the present analysis is consistent with, but slightly higher than, the value obtained by S96. However, it should be noted that, unlike the S5 0836+71 case, the extra-absorption is not very large in this source ($\Delta N_{\rm H} \sim 4 \times 10^{20}$ cm^{-2} in S96, $\Delta N_{\rm H} \sim 6 \times 10^{20}$ cm^{-2} in the present analysis) and could, therefore, be affected by the SIS calibration uncertainties discussed in §3.2 and Appendix B.

5. Discussion

5.1. Excess Absorption

The most striking result obtained from the present analysis is that the X-ray spectra of 5 high-z RLQs examined here are absorbed by column densities significantly higher than the Galactic value. Moreover, since these measurements correspond to the higher signal-to-noise data, they suggest that absorption is common (maybe ubiquitous) in high-z RLQs. In this section, we discuss the possible origin for such absorption.

5.1.1. Line-of-Sight Absorption

a) Galactic

Assuming that the extra absorption originates somewhere between the observer and the quasars, the first thing to examine is whether all of it could be produced in our Galaxy. This evaluation is commonly done through radio measurements at 21 cm which have been found to reasonably well trace the total amount of gas in the Galaxy (Dickey & Lockman 1990). However, the column densities are derived from measurements averaged over fairly large areas (several tens of arcmin^2). Moreover, radio observations only detect interstellar atomic hydrogen and neither molecular gas (e.g. H_2, CO, OH, etc.) nor dust. So it may happen that, for a given path, the total effective absorbing column is significantly higher than that indicated by 21 cm measurements. If one also considers the proper motion of molecular clouds, it could well be possible to explain strong and variable absorption by means of special conditions in our Galaxy alone. A remarkable example is the case of NRAO 140 which is located at the edge of a molecular cloud (the IC 348 cloud in the Perseus-Taurus region, Ungerechts & Thaddeus 1987). As discussed above (§4.3), when the molecular content along the line of sight is properly taken into account through ^{12}CO measurements to calculate the total effective absorption column, it is possible to account for the large X-ray absorption column measured for this quasar. Under this hypothesis, the absorption variability may plausibly be due to the passage of absorbing clouds across the line-of-sight. Given this possibility, we checked for Galactic CO emission in the direction of all quasars of the present sample (Table 7). Surveys of local CO emission toward extra-galactic sources did not detect CO emission in the direction of S5 0836+71 and PKS 2149-306 (Liszt & Wilson 1993, Liszt 1994). A deep (rms $\sim$ 0.04 K) observation in the direction of PKS 2126-158 puts another limit on any contribution from Galactic absorption in this source (Hartmann, private communication). From Table 7, note that S5 0014+81 is the source with the lowest Galactic latitude after NRAO 140 which increases the probability for a contamination from Galactic molecular clouds. Furthermore, S5 0014+81 is located at the edge of a large molecular cloud complex (the Polaris Flare) and CO emission is detected from positions nearby the quasar (e.g. from a point of local maximum at l=120.50 and b=18.63) over an area of more than 1 deg^2 (Heithausen et al. 1993). It is difficult to precisely quantify the contribution of the cloud to the total column density along the line of sight to S5 0014+81. However, we believe it is probably negligible in this case because from the CO emission map shown in Fig. 5 of Heithausen et al. (1993), the CO line intensity should be $\lesssim$ 0.4 K km s^{-1} in the direction of S5 0014+81. A rather conservative assumption for the CO-to-H_2 conversion factor of $\simeq$ 2–3 $\times$ 10^{20} molecules cm^{-2}K^{-1}km^{-1}s (Strong et al. 1988) would yield a column density $N_{\rm H_2} \simeq 1.6 \times 10^{20}$ atoms cm^{-2}, which is in any case negligible if compared to the atomic hydrogen column density of $N_{\rm H} \simeq 13.9 \times 10^{20}$ atoms cm^{-2} derived from 21 cm observations (Dickey & Lockman 1990).

Another indirect tracer of the total column of gas along a given path is the emission in the infrared band, in particular at 100 μm. The *IRAS* survey has shown that the Galactic IR emission is composed of a diffuse background emission plus several large, filamentary "cirrus" features (Low et al. 1984) predominantly associated to dust in clouds with column densities of a few $\times$ 10^{20} cm^{-2}, and located even at high Galactic latitudes. Using the *IRAS* Faint Source Survey catalog provided on-line (Moshir 1989) the IR emission within a radius of 6′ of each quasar was investigated (Table 7). There is no evidence for contamination from cirrus clouds in these quasars, except for PKS 2126-158 for which the *IRAS* Faint Source Survey maps indicate a probable contamination (Wheelock et al 1994). From the *IRAS* maps, the 100 μm flux in the direction of PKS 2126-158 is estimated to be $\lesssim$ 1.9 Jy (the

maximum value in that region) which corresponds to a brightness $\lesssim 1.5$ MJy sr^{-1} for a typical *IRAS* source covering $3' \times 5'$. Adopting a conservative range of $dS_{100}/dN_H \sim 0.5$–2.0 MJy sr^{-1}/10^{20} cm^{-2} (Reach , Heiles, & Koo 1993, Heiles, Reach, & Koo 1988, de Vries et al. 1987) as typical dust-to-gas ratios, this implies a total (H_2 + HI) hydrogen column density of 0.7–3×10^{20} cm^{-2}. These values are close to the 21 cm estimate of $N_H \simeq 4.85 \times 10^{20}$ cm^{-2} (Elvis et al. 1989), thus ensure that there is no significant excess IR emission and therefore that cirrus contamination is likely to be negligible for the present discussion even in this case.

In summary, on the basis of the above local CO properties and IR emission in the direction of these quasars, it is unlikely that all the extra absorption measured in X-rays is attributable to absorption by molecular clouds in our Galaxy, except possibly for NRAO 140. However, some contamination from molecular clouds and cirrus clouds may be present in S5 0014+81 and PKS 2126-158 respectively, but at a low level.

b) Extra-galactic

It has been known for decades that the space density of quasars decreases above z$\sim$3 (see Shaver et al. 1995 for a review). Though one plausible explanation for this decrease may be related to the way quasars evolve, it has also been argued that dust and gas in intervening galaxies could explain or at least contribute to the apparent turnover in space density (Ostriker & Heisler 1984). Examples of probable intervening galaxies have already been found in several high-z BL Lac objects (PKS 1413+135: Stocke et al. 1992; AO 0235+164: Madejski 1994; PKS 0537-44 and W1 0846+561: Narayan & Schneider 1990; MS 0205.7+3509: Stocke, Wurtz & Perlman 1995). Interestingly, soft X-ray absorption is often present at a level of $\sim$ few $\times 10^{21}$ cm^{-2}, which is similar to our findings.

A related possibility is absorption by gas and/or dust in damped Lyα systems (e.g. Fall & Pei 1993, 1995) which are plausibly associated to galaxy progenitors along the line of sight (Wolfe 1995). As extensively discussed by Elvis and collaborators in a variety of papers (E94 and references therein) which included three of the present quasars (PKS 0438-436, PKS 2126-158 and S5 0014+81), the numbers and column densities of intervening damped Lyα systems (Lanzetta et al. 1995) could possibly explain the measured X-ray absorption. It should be noted, however, that if the hypothesis of the intervening absorber is correct, whatever it is a galaxy or a damped Lyα system, it predicts that the absorption should remain constant over long time-scales. This is in apparent contrast with our findings where significant absorption variability has been detected in S5 0836+71 (§4.6) **though this "blazar-type" object may be intrinsically different from the other quasars.** Moreover, an absorption edge has been marginally detected in S5 0014+81 at the energy expected if the absorber is at the quasar redshift. These results suggest that the absorption is more likely intrinsic to the quasars, as discussed in the following.

5.1.2. Intrinsic Absorption

a) Absorption by dust and/or neutral gas

Recent observations are reviving the long-standing idea (Rieke, Lebofsky & Kinman 1979, Sanders et al. 1989) that quasars themselves may be embedded in large quantities of dust or thick gas. Webster et al. (1995) have recently **claimed** that a large population of radio-loud quasars are so red that they may have been missed by optical searches. This reddening is interpreted as arising from dust which is most likely located within the quasar host galaxy since the effect appears to be independent of redshift. Other evidence for obscuration have been found in several type 2 AGNs, including several narrow line radio galaxies of low and high luminosities (e.g. Cen A: Bailey et al. 1986; **3C 109: Goodrich & Cohen 1992, Allen & Fabian 1992;** Cygnus A: Ueno et al. 1994; 3C 265: Dey and Spinrad 1996). In these objects, the absorption is thought to arise in a nuclear torus, with a wide range of column densities (up to $N_H \sim 10^{24-25}$ cm^{-2}). These arguments argue in favor of the presence of large quantities of obscuring material, possibly in the form of dust. Other indirect evidence for large quantities of matter in high-z objects comes from the recent measurement by Ohta et al. (1996) of a strong CO (5-4) emission line from a z=4.69 radio-loud quasar. Assuming a Galactic CO-to-H_2 ratio, they infer a total mass of cold gas $\sim 10^{11}$ $M_\odot$.

Another possibility for the site of neutral absorbing material is in a cluster of galaxies. Since RLQs at z>0.5 are sometimes located in rich clusters of galaxies (Yee & Ellingson 1993), cluster cooling flows may provide the necessary cold material to produce the observed X-ray absorption (White et al 1991, E94). The radio galaxy Cygnus-A is a remarkable example of such scenario (Reynolds & Fabian 1996). However, again, **if the variable absorption observed in S5 0836+71, and possibly PKS 2149-306 is real, this could not be explained either by an absorption torus nor by a cooling flow model.** Thus an alternative explanation must be found, at least for these cases. One possible explanation could be the passage of neutral material (e.g. dense absorbing clouds) across the radiation field (possibly anisotropic). On one hand, cold clouds or "blobs" are expected to survive the intense radiation field close to the central regions of AGNs (Guilbert & Rees 1988, Celotti, Fabian & Rees 1992) and may well imprint reflection features (iron line and hard tail) commonly seen in the X-ray spectra of AGNs (Nandra & George 1994). On the other hand, anisotropic radiation, possibly with beam-

ing of the radiation, may be expected in these objects on the basis of the extremely high luminosity ($L_{2-10keV} \sim 10^{47-48}$ erg s^{-1}, in the quasar frame) observed and on the basis of general arguments on the unification of radio-loud quasars (Urry & Padovani 1995). As far as S5 0836+71 is concerned, superluminal radio components (Krichbaum et al. 1990), a rapid γ-ray flare observed by *EGRET* (von Linde et al. 1993), and theoretical arguments (Dondi & Ghisellini 1995) support the hypothesis that, at least in this object, the radiation source is relativistically beamed. Optically thin clouds with column densities of $N_H \sim 10^{21-23}$ cm^{-2} covering the continuum radiation or, alternatively, optically thick ($N_H > 10^{25}$ cm^{-2}) clouds covering quite a large fraction of it could plausibly reproduce the observed X-ray absorption. The variability could arise from the passage of the clouds across the radiation field line of sight.

b) Absorption by ionized gas

The absorption may also be produced by partially ionized "warm" material. Warm absorbers have been previously invoked to explain the complex X-ray absorption observed in several active galaxies (Nandra & Pounds 1994; Cappi et al. 1996) and quasars (**MR 2251-178: Halpern 1984, Otani 1996; 3C 351: Fiore et al. 1993, Mathur et al. 1994a; 3C 212: Elvis et al. 1994d, Mathur 1994b**). The state of a warm absorber depends only, though critically, on the ionization parameter, $\xi = L/nR^2$ (Kallman & McCray 1982). Since warm absorbers have been unambiguously detected in low luminosity AGNs, they may survive also at higher luminosities since, for a given density, the gas may just be at a larger distance from the central source. **As shown in §3.3.2, the present data are consistent with a warm absorber model as a possible explanation of the low energy absorption. However, the quality of the data coupled with the high redshifts do not allow to distinguish between a cold and ionized absorber.** It is interesting to note that if the *ASCA* X-ray spectrum of MR 2251-178, which clearly indicates the presence of a warm aborber ($\xi \simeq 28$, $N_{warm} \simeq 2.6 \times 10^{21}$ cm^{-2}), is redshifted to z=2 (i.e. the data are cut at $E \gtrsim 1.2$ keV), then it could be equally well fitted with a neutral absorption column density of $\sim 6\text{–}12 \times 10^{20}$ cm^{-2} (Otani, private communication), similar to what we find in our sample. This implies that the data accumulated to date for high-z quasars can hardly be used to distinguish between a cold or ionized absorber. A warm absorber cannot, therefore, be ruled out.

If the warm absorber hypothesis is correct, variable absorption could be interpreted as variation in the ionization state of the absorber (e.g., MCG-6-30-15: Fabian et al. 1994). An ionized absorber also predicts an absorption edge at E > 7.1 keV which seems to be at variance with our findings for S5 0014+81 where the fitted energy of the absorption edge is centered at ~ 7.1 keV. The quality of the data, however, does not exclude mildly ionized absorption either.

5.2. Statistical Properties

Correlations among the following parameters: photon index, column densities, 2–10 keV luminosity, radio-loudness, and source redshift have been searched for in the whole *ASCA* sample. The analysis shows no significant correlation which is unsurprising given the small size of the sample. Though not adequate for statistical correlations, the sample is, however, large enough to be representative of the entire class of high-z RLQs and as such, can be compared with other studies on statistical basis.

Earlier X-ray spectra of RLQs, mostly at low redshift, showed mean photon indices between $\sim 1.4\text{–}1.8$ both in the soft $\sim 0.1\text{–}4$ keV (*Einstein* IPC: Wilkes & Elvis 1987; *ROSAT* PSPC: Brunner et al. 1994) and hard $\sim 2\text{–}10$ keV (*EXOSAT*: Comastri et al. 1992; *Ginga*: Lawson & Turner 1996) energy bands. In some works, significant dispersion around the mean has been found (Brunner et al. 1994, Lawson & Turner 1996). If real, this indicates that either RLQs have an intrinsic dispersion of slopes or the intrinsic X-ray spectrum is more complex than a single absorbed power law (e.g. soft-excess or complex absorption). Previous X-ray spectra of high-z RLQs taken with *ROSAT* (E94, Bechtold et al. 1994b) and *ASCA* (Serlemitsos et al. 1994, S96) are consistent with an average photon index between $\sim 1.5\text{–}1.8$ up to 30 keV in the source frame.

The mean photon index derived for the whole sample over the full *ASCA* energy band is $< \Gamma_{0.5-10keV} > \simeq 1.61 \pm 0.04$ with a dispersion $\sigma_{0.5-10keV} \simeq 0.10 \pm 0.03$. **Excluding s5 0836+71 ??????** This average value is in agreement with most of the findings described above for low-z and high-z RLQs derived in both the soft and hard band, and indicates that there is no X-ray spectral evolution with redshift or luminosity over a broad $\sim 1\text{–}40$ keV energy band (source frame). This is further illustrated in Fig. 3 which shows the X-ray spectral slopes observed with *ASCA* between $\sim 0.5\text{–}10$ keV as a function of redshift and 2–10 keV luminosity (quasar frame) together with the photon indices obtained with *Ginga* for 18 low-z RLQs as reported by Lawson & Turner (1996). It is interesting to note that the dispersion is significantly different from zero also at high-z, though it is somewhat smaller than the *Ginga* value $\sigma \simeq 0.19^{+0.06}_{-0.04}$ (Lawson & Turner 1996). However, the mean photon index obtained with *ASCA* in the 2–10 keV energy band, where the present measurements are not affected by the absorption, is $< \Gamma_{2-10keV} > \simeq 1.53 \pm 0.05$, with a dispersion $\sigma_{2-10keV} \lesssim 0.12$. **Excluding s5 0836+71 ??????** The intrinsic dispersion is, in this case, consistent with zero within 1σ. This result implies that the above non-zero dispersion is probably a

consequence of the heterogeneous absorption measured in the data and that the intrinsic distribution of photon indices is well characterized by a single slope.

5.3. Implications for the XRB and GRB

It is by now widely accepted that AGNs could supply the bulk of the XRB emission above a few keV. Detailed modeling, based on the unified scheme and assuming the existence of a large population of absorbed AGNs, provide a good fit to the observed XRB spectrum up to $\sim$ 100 keV (Madau, Ghisellini & Fabian 1994; Comastri et al. 1995). If the absorption discovered in some of the objects in our sample turns out to be a common property of high-z, high-luminosity RQQs this would give a strong support to the above models.

It should be noted that RLQs constitute only a small fraction of the quasar population so that their contribution to the XRB is of the order of a few percent. This point is also enforced by our findings that the observed X-ray spectra of RLQs have $\Gamma \sim 1.5 - 1.6$ up to $\sim$ 40 keV in the source frame, steeper than the XRB as illustrated in Fig. 3. But the derived mean slope for the present sample has interesting implications for the γ-ray background. In fact, it has been recently pointed out (Comastri, Di Girolamo & Setti 1996) that flat spectrum radio quasar (FSRQ) may provide a significant fraction ($\sim$ 70–80 %) of the γ-ray background above several tens of MeV. This result has been achieved assuming that the X-ray spectra of FSRQ in the X-ray band (from $\sim$ 1 keV up to several hundreds of keV) are characterized by a slope with $\Gamma = 1.5$. Our findings provide, therefore, further support for this model suggesting that RLQs are likely to provide an important contribution to the hard X-ray – γ-ray backgrounds.

6. Conclusions

The present analysis of *ASCA* and *ROSAT* observations of high-z RLQs confirms that excess absorption is common in these objects. It is indeed detected significantly in the six brightest quasars of our sample. Unfortunately, even combining the two instruments, it is not possible to constrain the redshift of the absorber through direct spectral fitting. However, new results for S5 0836+71, and possibly S5 0014+81, favor the hypothesis that, at least in these two cases, the absorption is intrinsic to the quasars. Indeed, a comparison of *ASCA* and *ROSAT* spectra indicates the absorption has varied ($\Delta N_{\rm H} \sim 8 \times 10^{20}$ cm^{-2}) in S5 0836+71 on a time-scale of $\sim$ 2.4 yrs (observer frame) and an Fe K absorption edge is marginally detected in the *ASCA* observations of S5 0014+81, at the energy expected if the absorber is at the quasar's redshift. If we assume that the absorption is intrinsic for all objects in the sample, the column densities implied range between $\sim$ (1.7–55) $\times$ 10^{21} cm^{-2}.

Since the data do not allow to constrain unambiguously the redshift of the absorption, several possible origins have been considered. A careful search for Galactic CO and/or IR (100 μm) emission in the direction of the quasars indicates that the contribution to the total X-ray absorption column from molecular gas and dust present in our Galaxy is negligible for the majority of the quasars. It is, however, likely to be significant in the case of NRAO 140. Extra-galactic absorption from intervening galaxies and/or damped Lyα systems may be relevant for some of the objects, but is not consistent with the new findings for S5 0836+71 and S5 0014+81. Intrinsic absorption from an absorption torus or intracluster gas is also unlikely in the light of the absorption variability. It is argued, therefore, that the preferable explanation is intrinsic absorption by cold gas, possibly in the form of clouds, near the central source. A warm absorber would be a plausible candidate as well.

The accumulated counts allowed us to put, **for most objects, stringent** limits on the presence of an Fe K emission line, with upper limits on the EW ranging between $\sim$ 40–400 eV in the quasar frame. Alternative continuum models have also been fitted to the data. The upper limits on the intensity of Compton reflection range between R $\sim$ 0.1–0.7. A broken power law model, tested as an alternative explanation for the low energy cut-off, would require unreasonably flat ($\Gamma < 1$) slopes at low energies, though it cannot be ruled out by the data. It is also argued that a thermal bremsstrahlung origin for the observed continuum is unlikely.

The average photon index ($< \Gamma > \sim 1.5$–1.6) is consistent with previous measurements at high and low-z, therefore suggesting that RLQs do not show spectral changes over about two decades in energy ($\sim$ 0.4–40 keV) with either redshift or luminosity. This average slope, which is steeper than the spectrum of the XRB but flatter than the average slopes of RQQs and low-luminosity AGNs, also suggests that RLQs do not contribute significantly to the XRB but, instead, are likely to provide a significant fraction of the γ-ray background flux.

APPENDICES

A. GIS Backgrounds

In the standard way of analyzing *ASCA* GIS spectra, there are two possible choices for the background subtraction: either from a source-free part of the observation field of view (hereafter "local background"), or from the available blank sky observations with the same region filter as used for the source spectrum (see "The ABC Guide to *ASCA* Data Reduction"). Both methods should, in principle, give similar results. However, slight but significant differences in the source spectral slopes were found in the present analysis and forced us

to choose a non-standard background region.

The problem is that background regions extracted from the source field of view almost inevitably fall at a substantial off-axis distance because sources are usually pointed nearly on-axis. But as the distance from the X-ray telescope optical axis increases, reduction of the contribution from the cosmic X-ray background (due to the vignetting) and softening of the non X-ray background (Kubo et al. 1994) change in a complex and position dependent manner the spectrum of the background, which cannot be corrected in the current analysis procedure. On the other hand, standard background regions extracted from the blank sky files from the same area as that used for the source almost always include the regions contaminated by the Seyfert 2 galaxy NGC 6552 (Ebisawa 1994). Because of the very strong Fe K emission line of this source at $\sim$ 6.4 keV (Fukazawa et al. 1994), the source spectra obtained with blank sky backgrounds tend to be steeper than those obtained with local background subtractions. As a result, in the analysis of the weakest sources (typically those with intensity $\lesssim$ 0.1 cts/s), different backgrounds often yielded significantly different source slopes with deviations up to $\Delta\Gamma \sim 0.2$. Therefore, we adopted a non-standard background extracted from the GIS standard blank sky files from a region non contaminated by NGC 6552 and at the same or, if not possible, similar off-axis distance of the source region. This choice of background has the advantage to avoid the above problems of the off-axis position with the local background and of the contamination by NGC 6552 with the blank sky background. However, it has the disadvantage that the screening criteria of the blank sky background never match exactly those of the source observation (similarly to any other choice of blank sky background). However, we estimate this is a minor problem when standard screening criteria are adopted because the GIS background reproducibility (in time) is achieved with systematic errors less than a few percent (Ikebe et al. 1995).

B. On the *ASCA* SIS response uncertainties at low energies

Although the results obtained with *ASCA* and *ROSAT* always agree within their statistical errors (except for S5 0836+71), the present analysis indicates that the *ASCA* spectra require systematically more absorption than the *ROSAT* spectra (Fig. 1). This suggests that the SIS responses may suffer of a systematic excess absorption, though *ROSAT* PSPC calibration uncertainties (e.g. non-linear gain variations) may play a role as well. This confirms previous, more detailed, studies on the SIS calibration uncertainties at low energies (e.g. Hayashida et al. 1995). Indeed, it is widely recognized that there are local features around 0.5–0.6 keV which show up, preferentially in strong sources, in the form of absorption edges around 0.5 keV and/or emission lines at $\sim$ 0.6 keV (e.g. Guainazzi & Piro 1994, Cappi et al. 1996). The origin of the problem is not clear, though probably related to the presence of the Oxygen K-edge (produced in the CCD dead layer) at E $\simeq$ 0.54 keV in the SIS response. Because of this edge, a small offset and/or variations of a few eV in the exact response energy scale could easily be responsible for such features. Though no clear feature is evident in the low energy residuals of the quasars spectra (Fig. 2), it is possible that it could have affected somehow our measurements. Other uncertainties concern the absolute SIS efficiency at low energies which is currently being quantified in terms of a systematic error of $\sim 3 \times 10^{20}$ cm^{-2} for SIS0 and $\sim 2 \times 10^{20}$ cm^{-2} for SIS1 in the absorption column (Hayashida et al. 1995). This problem is probably related to the correct calibration of the SIS quantum efficiency, i.e. the thickness of the CCD dead layer. It is not clear, however, how much the above local features at E $\sim$ 0.5 keV are responsible for and/or related to such excess absorption but, in principle, both effects (local features and excess absorption) should be already taken into account in the systematic error of $\sim 3 \times 10^{20}$ cm^{-2}.

In light of the above considerations, we have performed a series of checks in order to establish the reliability of the measured excess absorption for all *ASCA* spectra.

a) Test 1 - Artificial gain shifts:

Using the "gain" command in XSPEC, we shifted the energy scales of the SIS0 and SIS1 responses between $\pm$ 20 eV, i.e. within the typical systematic 2σ uncertainties in the energy scale (Otani & Dotani 1994). The observed changes in the column densities were, in every case, lower than 2×10^{20} cm^{-2}, which is smaller than the typical statistical errors found in the present work.

b) Test 2 - Cut of the data below 0.65 keV:

When, more drastically, all data below 0.65 keV were ignored, the fits yielded even larger best-fit absorption columns for the quasars NRAO 140, PKS 0438-436, PKS 0537-286 and PKS 2126-158. For S5 0014+81 and S5 0836+71, the columns were lowered by $\sim 1 \times 10^{20}$ cm^{-2} ($\sim$ 5%) and $\sim 2.5 \times 10^{20}$ cm^{-2} ($\sim$ 20%), respectively. In every case, the absorption columns remained significantly higher than the Galactic value at more than 99% confidence level.

From a) and b), we conclude that the measured SIS excess absorption cannot be attributed to the local detector features commonly reported around 0.5–0.6 keV. The problem is more likely related to the SIS efficiency as a whole at low energies.

c) Test 3 - Comparison with the calibration source 3C 273:

The SIS response matrices were calibrated on the ground and then cross-calibrated with the GIS in-flight

using the observations of the quasar 3C 273. In particular, the response matrices of SIS0 chip number 1 and SIS1 chip number 3 (the chips used in the present analysis) were calibrated using an observation performed in 1993, December 20th. The calibrations were performed taking the slopes from the GIS spectra and assuming Galactic absorption. 3C 273 was observed 8 more times by *ASCA*. Results obtained from the overall observations (Cappi & Matsuoka 1996) do not modify the conclusions presented below. For the purpose of investigating the efficiency of the SIS, only the results from the December 20th 1993 calibration observation are reported below. The observation was analyzed using the same criteria (same screening criteria, extraction regions, etc.) used for the quasars to allow a direct comparison. About 82 000 counts/SIS were collected in the 0.4–10 keV energy range, for a total exposure time of $\sim$ 15 500 s. The spectra extracted for SIS0 and SIS1 were then fitted with a single absorbed power law, first separately and then simultaneously. Confidence contours obtained from each fit are shown in Fig. 4. The best-fit column density is larger than the Galactic column in both SIS0 and SIS1, yielding an excess column density of $\sim 2 \times 10^{20}$ cm^{-2} in the fit with both detectors. This value gives a direct estimate of the systematic error we must take into account when interpreting the results from the present analysis. This estimate is in good agreement with the measurements obtained by Hayashida et al. (1995). Also, it should be noted that independent analysis of the SIS data extracted from the central regions of Coma cluster also show excess absorption of $\sim 3 \times 10^{20}$ cm^{-2} (Hashimotodani, private communication).

Therefore, we conclude that the total systematic error of the absorption column density should be *conservatively* smaller than $\sim$ 3–4 $\times$ 10^{20} cm^{-2}. In the analysis presented in §3 and when discussing the results, only deviations larger than this value have been considered.

ACKNOWLEDGMENTS

The authors would like to thank all the *ASCA* team members for making these observations possible. M.C. thanks all his colleagues in RIKEN for helpful discussions and Dr. Dap Hartmann for measuring the Galactic CO emission in the direction of PKS 2126-158. M.C. also acknowledges financial support from the Science and Technology Agency of Japan (STA fellowship), hospitality from the RIKEN Institute and support from the European Union. G.G.C.P. acknowledges partial financial support from MURST and ASI. A.C. acknowledges financial support from the Italian Space Agency under the contracts ASI-94-RS-96 and ASI-95-RS-152. This work has made use of the NASA/IPAC Extragalactic Database (NED) which is operated by the Jet Propulsion Laboratory, Caltech, under contract with the National Aeronautics and Space Administration.

REFERENCES

Allen, S.W., & Fabian, A.C., 1992, MNRAS, 258P, 29

Anders, E., & Grevesse, N., 1989, Geochimica et Cosmochimica Acta, 53, 197

Arnaud, K.A., Haberl, F., & Tennant, A., 1991, XSPEC User's Guide, ESA TM-09

Bailey, J., Sparks, W.B., Hough, J.H., & Axon, D.J., 1986, Nature, 322, 150

Bania, T.M., Marscher, A.P., & Barvainis, R., 1991, AJ, 101, 2147

Barr, P., Giommi, P., & Maccagni, D., 1988, ApJ, 324, L11

Bechtold, J., et al., 1994, AJ, 108, 374

Brinkmann, W., Siebert, J., & Boller, T., 1994, A&A, 281, 355

Brunner, H., Friedrich, P., Zimmermann, H., & Staubert, R., 1992, in "X-ray emission from Active Galactic Nuclei and the Cosmic X-ray Background", Ed. W. Brinkmann & J. Trümper (MPE Report 235), p198

Brunner, H., Lamer, G., Worrall, D.M., & Staubert, R., 1994, A&A, 287, 436

Bühler, P., Courvoisier, T.J.-L., Staubert, R., Brunner, H., & Lamer, G., 1995, A&A, 295, 309

Cappi, M., Mihara, T., Matsuoka, M., Hayashida, K., Weaver, K.A., & Otani, C., 1996, ApJ, 458, 149

Cappi, M., & Matsuoka, M., 1996, in the Proceedings of "X-ray Imaging and Spectroscopy of Cosmic Hot Plasmas", Waseda University, Tokyo

Celotti, A., Fabian, A.C., & Rees, M.J., 1992, MNRAS, 255, 419

Comastri, A., Setti, G., Zamorani, G., Elvis, M., Giommi, P., Wilkes, B.J., & McDowell, J.C., 1992, ApJ, 384, 62

Comastri, A., Setti, G., Zamorani, G., & Hasinger, G., 1995, A&A, 296, 1

Comastri, A., Cappi, M., & Matsuoka, M., 1996, in Proc. Röentgenstrahlung from the Universe, Würzburg, Germany, Ed. H.-U. Zimmermann, J.E. Trümper & H. Yorke, MPE Report 263, in press

Comastri, A., Di Girolamo, T., & Setti, G., 1996, A&ASupplement Series, in press

Dey, A., & Spinrad, H., 1996, ApJ, 459, 133

de Vries, H.W, Heithausen, A., & Thaddeus, P., 1987, ApJ, 319, 723

Dickey, J.M. & Lockman, F.J., 1990, ARA&A, 28, 215

Dondi, L., & Ghisellini, G., 1995, MNRAS, 273, 583

Ebisawa, K., 1994, GOF Report

Elvis, M., Lockman, F.J., & Wilkes, B.J., 1989, AJ, 97, 777

Elvis, M., et al., 1994a, ApJS, 95, 1

Elvis, M., Fiore, F., Wilkes, B., McDowell, J.C., & Bechtold, J., 1994b, ApJ, 422, 60 (E94)

Elvis, M., Matsuoka, M., Sieminginowska, A., Fiore, F., Mihara, T., & Brinkmann, W., 1994c, ApJ, 436, L55

Elvis, M., Fiore, F., Mathur, S., & Wilkes, B., 1994d, ApJ, 425, 103

Fabian, A.C., et al., 1994, PASJ, 46, L59

Fall, S.M., & Pei, Y.C., 1993, ApJ, 402, 479

Fall, S.M., & Pei, Y.C., 1995, in "QSO Absorption Lines", Ed. G. Meylan, (Springer-Verlag: Heidelberg), p23

Feldman, U., 1992, Physica Scripta, 46, 202

Fiore, F., Elvis, M., Mathur, S., Wilkes, B.J., & McDowell, J.C., 1993, ApJ, 415, 129

Fukazawa, Y., et al., 1994, PASJ, 46, L141

Gendreau, K.C., et al., 1995, PASJ, 47, L5

Goodrich, R.W., & Cohen, M.H., 1992, ApJ, 391, 623

Guainazzi, M., & Piro, L., 1994, RIKEN report

Guilbert, P.W., & Rees, M.J., 1988, MNRAS, 233, 475

Halpern, J.P., 1984, ApJ, 281, 90

Hayashida, K., Miura, N., Hashimotodani, K., & Murakami, S., 1995, ISAS Internal Report

Heiles, C., Reach, W.T., & Koo, B.-C., 1988, ApJ, 332, 313

Heithausen, A., Stacy, J.G., de Vries, H.W., Mebold, U., & Thaddeus, P., 1993, A&A, 268, 265

Ikebe, Y., Ishisaki, Y., Kubo, H., Idesawa, E., Takahashi, T., & Makishima, K., 1995, *ASCA* News n. 3

Kallman, T.R., & McCray, R., 1982, ApJS, 50, 263

Krichbaum, T.P., Hummel, C.A., Quirrenbach, A., Schalinski, C.J., & Witzel, A., 1990, A&A, 230, 271

Krolik, J.H., & Kallman, T.R., 1984, ApJ, 286, 366

Kubo, H., Ikebe, Y., & Makishima, K., et al., 1994, *ASCA* News n.2, 14

Lanzetta, K.M., Wolfe, A.M., & Turnshek, D.A., 1995, ApJ, 440, 435

Lawson, A.J., Turner, M.J.L., Williams, O.R., Stewart, G.C., & Saxton, R.D., 1992, 259, 743

Lawson, A.J., & Turner, M.J.L., 1996, MNRAS, submitted

Leahy, D.A., & Creighton, J., 1993, MNRAS, 263, 314

Lightman, A.P., & White, T.R., 1988, ApJ, 335, 57

Liszt, H.S., & Wilson, R.W., 1993, ApJ, 403, 663

Liszt, H.S., 1994, ApJ, 429, 638

Low, F.J., et al., 1984, ApJ, 278, L19

Maccacaro, T., Gioia, I.M., Wolter, A., Zamorani, G., & Stocke, J.T., 1988, ApJ, 326, 680

Madau, P., Ghisellini, G., & Fabian, A.C., 1994, MNRAS, 270, L17

Madejski, G., 1994, ApJ, 432, 554

Magdziarz, P., & Zdziarski, A.A., 1995, MNRAS, 273, 837

Makishima, K., 1986, Lecture Notes in Physics (Springer Verlag: Berlin), 266, 249

Marscher, A.P., 1988, ApJ, 334, 552

Mathur, S., Wilkes, B., Elvis, M., & Fiore, F., ApJ, 434, 493

Mathur, S., 1994b, ApJ, 431, L75

Morrison, R., & McCammon, D., 1983, ApJ, 270, 119

Moshir, M., 1989, *IRAS* Faint Source Catalog Explanatory Supplement, IPAC preprint 44

Mushotzky, R.F., Done, C., & Pounds, K.A., 1993, ARA&A, 31, 717

Nandra, K. & George, I.M., 1994, MNRAS, 267, 974

Nandra, K., & Pounds, K.A., 1994, MNRAS, 268, 405

Nandra, K., Fabian, A.C., Brandt, W.N., Kunieda, H., Matsuoka, M., Mihara, T., Ogasaka, Y., & Terashima, Y., 1995, MNRAS, 276, 1

Narayan, R., & Schneider, P., 1990, MNRAS, 243, 192

Nolan, P.L., et al., 1996, ApJ, 459, 100

Ohashi, T., Tashiro, M., Makishima, K., Kii, T., Makino, F., Turner, M.J.L., & Williams, O.R., 1992, ApJ, 398, 87

Ohta, K., et al., 1996, submitted to Nature

Ostriker, J.P., & Heisler, J., 1984, ApJ, 278, 1

Otani, C., & Dotani, T., 1994, *ASCA* News n. 2, 25

Otani, C., 1995, PhD Thesis, University of Tokyo

Otani, C., et al., 1996, in Proc. Röentgenstrahlung from the Universe, Würzburg, Germany, Ed. H.-U. Zimmermann, J.E. Trümper & H. Yorke, MPE Report 263, in press

Pfefferman, E., et al., 1987, Proc. SPIE, 733, 519

Reach, W.T., Heiles, C., & Koo, B.-C., 1993, ApJ, 412, 127

Rees, M.J., 1984, ARA&A, 22, 471

Reynolds, C.S., & Fabian, A.C., 1995, MNRAS, 273, 1167

Reynolds, C.S., & Fabian, A.C., 1996, MNRAS, 278, 479

Rieke, G.H., Lebofsky, M.J., & Kinman, T.D., 1979, ApJ, 232, L151

Sanders, D.B., Phinney, E.S., Neugebauer, G., Soifer, B.T., & Matthews, K., 1989, ApJ, 347, 29

Serlemitsos, P., Yaqoob, T., Ricker, G., Woo, J., Kunieda, H., Terashima, Y., & Iwasawa, K., 1994, PASJ, 46, L43

Shaver, P.A., 1995, in the Proceedings of the 17th Texas Symposium on Relativistic Astrophysics & Cosmology, Ed. H. Böhringer, G.E. Morfill & J.E. Trümper, 759, 87

Siebert, J., Matsuoka, M., Brinkmann, W., Cappi, M., Mihara, T., & Takahashi, T., 1996, A&A, 307, 8 (S96)

Steigman, G., 1994, MNRAS, 269, L53

Stocke, J.T., Wurtz, R.E., Wang, Q., Elston, R., & Jannuzzi, B., 1992, ApJ, 400, L17

Stocke, J.T., Wurtz, R.E., & Perlman, E.S., 1995, ApJ, 454, 55

Strong, A.W., Bloemen, J.B.G.M., Dame, T.M., Grenier, I.A., & Hermsen, W., 1988, A&A, 207, 1

Tanaka, Y., Inoue, H., & Holt, S.S., 1994, PASJ, 46, 37

Thompson, D.J., et al., 1995, ApJS, 101, 259

Trümper, J., 1983, Adv. Space Res., 2, 241

Turner, T.J., George, I.M., Madejski, G.M., Kitamoto, S., & Suzuki, T., 1995, ApJ, 445, 660

Ueno, S., Koyama, K., Nishida, M., Yamauchi, S., & Ward, M.J., 1994, ApJ, 431, L1

Ungerechts, H., & Thaddeus, P., 1987, ApJS, 63, 645

Urry, C.M., & Padovani, P., 1995, PASP, 107, 803

Véron-Cetty, M.-P., & Véron, P., 1993, European Southern Observatory, Scientific Report n. 13, 6^{th} Edition

von Linde, J., et al., 1993, A&A, 267, L23

Wamsteker, W., 1981, A&A, 97, 329

Webster, R.L., Francis, P.J., Peterson, B.A., Drinkwater, M.J., & Masci, F.J., 1995, Nature, 375, 469

Wheelock, S.L., et al., 1994, *IRAS* Sky Survey Atlas: Explanatory Supplement

White, D.A., Fabian, A.C., Forman, W., Jones, C., & Stern, C., 1991, ApJ, 375, 35

Wilkes, B.J., & Elvis, M., 1987, ApJ, 323, 243

Wilkes, B.J., Elvis, M., Fiore, F., McDowell, J.C., Tananbaum, H., & Lawrence, A., 1992, ApJ, 393, L1

Wilkes, B.J., Tananbaum, H., Worrall, D.M., Avni, Y., Oey, M.S., & Flanagan, J., 1994, ApJS, 95, 1

Williams, O.R., et al., 1992, ApJ, 389, 157

Wolfe, A.M., 1995, in "QSO Absorption Lines", Ed. G. Meylan, (Springer-Verlag: Heidelberg), p13

Yee, H.K.C., & Ellingson, E., 1993, ApJ, 411, 43

Zamorani, G., et al., 1981, ApJ, 245, 357

Zimmerman, H.U., Belloni, T., Izzo, C., Kahabka, P., & Schwentker, O., 1993, EXSAS User's Guide, MPE Report 244

This 2-column preprint was prepared with the AAS LaTeX macros v3.0.

TABLE 1: The Radio-Loud Quasar Sample

Object	R.A.[a] (J2000)	DEC.[a] (J2000)	z[a]	N_{Hgal}^{b} (10^{20} cm^{-2})	m_V^a	f_{5GHz}^a (mJy)	R_L^c
S5 0014+81	00 17 08.5	+81 35 08.1	3.38	13.9	16.5	551	2.78
PKS 0332-403	03 34 13.6	-40 08 25.4	1.44	1.43	18.5	2600	4.24
NRAO 140	03 36 30.1	+32 18 29.3	1.26	14.2*	17.5	2500	3.87
PKS 0438-436	04 40 17.2	-43 33 08.6	2.85	1.47	18.8	7580	4.84
PKS 0537-286	05 39 54.3	-28 39 56.2	3.10	1.95*	20.0	990	4.39
S5 0836+71	08 41 24.4	+70 53 42.2	2.17	2.78	16.5	2573	3.45
PKS 1614+051	16 16 37.5	+04 59 33.2	3.21	4.90	19.5	850	4.15
PKS 2126-158	21 29 12.2	-15 38 40.8	3.27	4.85*	17.0	1240	3.33
PKS 2149-306	21 51 55.5	-30 27 53.7	2.34	1.91	17.9	1150	3.66

[a] Coordinates, redshift, V magnitude and radio flux at 5 GHz, from Véron-Cetty & Véron (1993).

[b] Galactic absorption from Dickey & Lockman (1990). The values marked with (*) are from Elvis et al. (1989).

[c] Radio-Loudness defined as $R_L = \log(f_{5GHz}/f_V)$. We used $m_V(0)$=3360 Jy (Wamsteker W. 1981)

TABLE 2 : *ROSAT* Observation Log

Object	Date	Wobble	Matrix	Exposure (s)	NC[a]	Ref.[b]
S5 0014+81	03/15/91	on	DRM06	5951	394	1,2
NRAO 140	08/08/92	on	DRM36	4039	992	3
PKS 0438-436	02/19/91	off	DRM06	10725	645	1,4
PKS 0438-436	09/19/92	on	DRM36	10506	547	1
PKS 0537-286	09/28/92	on	DRM36	9487	568	5
S5 0836+71	03/23/92	on	DRM36	6993	5400	6
S5 0836+71	11/02/92	on	DRM36	5026	2008	6
PKS 2126-158	05/08/91	on	DRM06	3424	613	1,2
PKS 2126-158	11/12/92	on	DRM36	3968	729	1,2
PKS 2126-158	04/27/93	on	DRM36	4160	741	This work
PKS 2126-158	05/17/93	on	DRM36	1610	321	This work

[a] NC: Net counts.

[b] References: (1) E94, (2) Bechtold et al. (1994), (3) Turner et al. (1995), (4) Wilkes et al. (1992), (5) Bühler et al. (1995), (6) Brunner et al. (1994)

TABLE 3: *ASCA* Observations Log

Object	Date	Exposure[a] (s)		Count Rate[a] ($\times 10^{-2}$ s^{-1})		CCD mode	Ref.[b]
		GIS	SIS	GIS	SIS		
S5 0014+814 (AOI)	10/29/93	39004	21750	7.33	3.88	4 CCD	(1) + This work for SIS
S5 0014+814 (AOII)	10/07/94	27494	20703	5.14	5.98	1 CCD	This work
PKS 0332-403	08/12/94	16646	14153	1.98	2.65	1 CCD	(2)
NRAO 140	02/02/94	33181	32178	16.3	20.7	1 CCD	(3)
PKS 0438-436	07/13/93	34499	26412	2.77	3.20	4 CCD	(4)
PKS 0537-286	03/12/94	36236	29052	2.51	4.21	1+2 CCD	(2)
S5 0836+71	03/17/95	16532	10540	24.0	30.3	1 CCD	This work
PKS 1614+051	08/02/94	39695	32577	0.88	0.55	1 CCD	(2)
PKS 2126-158	05/16/93	15914	14291	10.1	12.8	1 CCD	(4)
PKS 2149-306	10/26/94	19168	16504	19.0	25.5	1 CCD	(2)

[a] Reported values for the GIS and SIS are averaged over the detectors (GIS2 with GIS3 and SIS0 with SIS1).

[b] References: (1) Elvis et al. (1994c), (2) S96, (3) Turner et al. (1995), (4) Serlemitsos et al. (1994)

TABLE 4 : *ROSAT* X-Ray Spectral Fits
PSPC - Single Power Law (N_H free)

Object	Energy Range[a] (keV)	N_H (10^{20} cm^{-2})	Γ	A_{pl}^b	χ^2_{red}/dof	F_{SX}^c	log L_{SX}^d
S5 0014+81	~0.4-10	$20.0^{+30.0}_{-15.2}$	$1.89^{+2.40}_{-1.03}$	5.30	1.37/17	0.73	47.8
NRAO 140	~0.2-5	$22.5^{+21.9}_{-14.0}$	$1.53^{+1.14}_{-0.81}$	20.7	1.21/15	2.88	46.9
PKS 0438-436 (Feb 91)	~0.4-9	$8.13^{+20.4}_{-3.69}$	$1.71^{+1.16}_{-0.48}$	3.53	0.45/19	0.71	47.3
.....(Sep 92)	"	$5.07^{+4.09}_{-2.23}$	$1.57^{+0.49}_{-0.44}$	2.51	1.28/25	0.57	47.0
.....(tot.)	"	$6.31^{+4.19}_{-2.04}$	$1.63^{+0.36}_{-0.32}$		0.93/46		
PKS 0537-286	~0.4-10	$3.11^{+1.84}_{-1.50}$	$1.50^{+0.45}_{-0.44}$	2.61	1.84/7	0.65	47.1
S5 0836+71 (Mar 92)	~0.3-7	$3.29^{+0.48}_{-0.46}$	$1.51^{+0.13}_{-0.12}$	35.0	1.27/18	8.59	47.8
.....(Nov 92)	"	$3.45^{+0.79}_{-0.80}$	$1.55^{+0.22}_{-0.22}$	17.9	1.55/18	4.41	47.5
.....(tot.)	"	$3.33^{+0.42}_{-0.41}$	$1.52^{+0.12}_{-0.11}$		1.34/38		
PKS 2126-158 (May 91)	~0.4-10	$8.38^{+13.7}_{-3.82}$	$1.44^{+0.81}_{-0.50}$	10.4	0.95/18	2.08	47.7
.....(Nov 92)	"	$9.01^{+22.8}_{-4.25}$	$1.50^{+1.22}_{-0.46}$	10.9	0.93/21	2.13	47.8
.....(Apr 93)	"	$7.23^{+8.27}_{-2.89}$	$1.51^{+0.57}_{-0.42}$	10.0	0.85/15	2.08	47.7
.....(May 93)	"	$11.5^{+37.6}_{-6.61}$	$1.91^{+2.07}_{-0.74}$	12.7	1.05/15	2.23	48.2
.....(tot.)	"	$8.42^{+4.88}_{-2.30}$	$1.53^{+0.34}_{-0.25}$		0.90/75		

Note: Intervals are at 90% confidence, for two interesting parameters.

[a] Approximate energy range, in the quasar rest frame.

[b] Unabsorbed flux at 1 keV (observed frame) in units of 10^{-4} photons cm^{-2} s^{-1} keV^{-1}.

[c] Absorbed flux between 0.1–2 keV (observed frame) in units of 10^{-12} ergs cm^{-2} s^{-1}.

[d] Intrinsic luminosity between 0.1–2 keV (quasar frame) in units of ergs s^{-1}.

TABLE 5: *ASCA* X-Ray Spectral Fits

GIS+SIS - Single Power Law ($N_{\rm H}$ free; $N_{\rm H} \equiv N_{\rm Hgal}$)

Object	Energy Range[a] (keV)	$N_{\rm H}$ (10^{20} cm^{-2})	Γ	$A^b_{\rm pl}$	χ^2_{red}/dof	$F^c_{\rm HX}$	$F^d_{\rm SX'}$	log $L^e_{\rm HX}$	EW (FeK)[f] (eV)	$\tau_{\rm edge}(FeK)$[g]
0014+81 (Oct 93)	~2–40	$28.4^{+6.2}_{-5.7}$	$1.75^{+0.09}_{-0.08}$	6.46	1.03/314	2.43	0.82	47.8	<75	<0.23
.....(Oct 94)	"	$26.9^{+6.9}_{-6.3}$	$1.66^{+0.10}_{-0.12}$	6.60	0.92/237	2.49	0.73	47.7	<131	$0.21^{+0.18}_{-0.17}$
.....(tot.)	"	$28.1^{+4.5}_{-4.2}$	$1.72^{+0.06}_{-0.07}$	—	1.02/553				<70	$0.15^{+0.12}_{-0.11}$
		13.9 Fixed	$1.54^{+0.03}_{-0.03}$	—	1.13/554					
PKS 0332-403	~1–20	< 22.9	$1.73^{+0.28}_{-0.25}$	2.48	0.77/103	0.94	0.47	46.3	<415	<0.66
		1.43 Fixed	$1.60^{+0.11}_{-0.12}$	2.05	0.78/104					
NRAO 140	~1–20	$31.8^{+3.0}_{-2.8}$	$1.70^{+0.05}_{-0.04}$	21.8	0.96/864	9.09	2.56	47.1	<36	<0.10
		14.2 Fixed	$1.46^{+0.02}_{-0.02}$	16.3	1.23/865					
PKS 0438-436	~2–38	$15.2^{+9.1}_{-7.7}$	$1.63^{+0.16}_{-0.14}$	3.89	0.93/236	1.75	0.63	47.3	<240[h]	<0.29[h]
		1.47 Fixed	$1.42^{+0.06}_{-0.06}$	2.92	1.00/237					
PKS 0537-286	~2–40	$7.5^{+6.4}_{-5.5}$	$1.46^{+0.14}_{-0.13}$	3.09	0.74/197	1.85	0.63	47.4	<139	<0.15[h]
		1.95 Fixed	$1.36^{+0.06}_{-0.06}$	2.71	0.76/198					
S5 0836+71	~1–30	$11.4^{+3.0}_{-2.8}$	$1.45^{+0.05}_{-0.05}$	23.3	0.87/503	14.0	4.25	47.8	<110	<0.11[h]
		2.78 Fixed	$1.32^{+0.03}_{-0.03}$	19.3	0.97/504					
PKS 1614+051[i]	~2–40	4.90 Fixed	1.6 Fixed	0.43		0.21[i]	0.10[i]	46.4[i]		
PKS 2126-158	~2–40	$13.6^{+5.3}_{-4.3}$	$1.68^{+0.09}_{-0.09}$	13.1	1.01/331	5.51	2.20	47.9	<107	<0.08
		4.85 Fixed	$1.53^{+0.04}_{-0.04}$	10.8	1.07/332					
PKS 2149-306	~1–30	$8.3^{+1.8}_{-2.2}$	$1.54^{+0.05}_{-0.05}$	19.2	1.07/633	9.94	3.81	47.8	<85[h]	<0.17[h]
		1.91 Fixed	$1.42^{+0.03}_{-0.02}$	16.3	1.13/634					

Note: Intervals are at 90% confidence, for two interesting parameters when $N_{\rm H}$ is free and for one interesting parameter when $N_{\rm H}$ is fixed at the Galactic value.

[a] Approximate energy range, in the quasar rest frame. [b] SIS unabsorbed flux at 1 keV (observed frame) in units of 10^{-4} photons cm^{-2} s^{-1} keV^{-1}. [c] Absorbed flux between 2–10 keV (observed frame) in units of 10^{-12} ergs cm^{-2} s^{-1}, calculated with the SIS normalization only. [d] Absorbed flux between 0.1–2 keV (observed frame) in units of 10^{-12} ergs cm^{-2} s^{-1}, extrapolated from the best-fit spectra (i.e. with the SIS normalization). [e] Intrinsic luminosity between 2–10 keV (quasar frame) in units of ergs s^{-1}, calculated with the SIS only. [f] 90% limit on the equivalent width of the Fe K line measured in the observer frame, with σ = 0 eV and E = 6.4 keV (quasar frame), for one interesting parameter ($\Delta\chi^2 = 2.71$). [g] 90% limit on the absorption edge depth with energy fixed at 7.1 keV (quasar frame). [h] Value affected by the calibration uncertainties of the SIS between ~ 1.8–2.4 keV. An estimated conservative systematic error of 10 eV (observer frame) for the lines and $\Delta\tau = 0.05$ for the edge depth have been added to these values. [i] Quasar was detected but with too few counts to perform a spectral analysis. Fluxes and luminosity are calculated assuming a photon index = 1.6 (i.e. the average value from the sample) and Galactic absorption.

TABLE 6: *ASCA* and *ROSAT* Combined Spectral Fits

A. Single Power Law ($N_{\rm H}$ free; $N_{\rm H}$ at z + $N_{\rm Hgal}$)

Object	Energy Range[a] (keV)	$N_{\rm H}$ (10^{20} cm^{-2})	Γ	χ^2_{red}/dof
S5 0014+81	~0.4–40	$27.4^{+4.0}_{-4.3}$	$1.71^{+0.06}_{-0.07}$	1.03/572
		554^{+196}_{-170}	$1.70^{+0.07}_{-0.06}$	1.02/572
NRAO 140	~0.2–20	$31.1^{+2.9}_{-2.7}$	$1.70^{+0.04}_{-0.05}$	0.97/881
		109^{+20}_{-19}	$1.66^{+0.05}_{-0.04}$	0.98/881
PKS 0438-436	~0.4–38	$5.81^{+2.66}_{-1.40}$	$1.48^{+0.10}_{-0.09}$	0.97/281
		$71.9^{+44.1}_{-22.2}$	$1.45^{+0.09}_{-0.09}$	0.97/281
PKS 0537-286	~0.4–40	$2.82^{+0.97}_{-0.74}$	$1.38^{+0.08}_{-0.08}$	0.77/204
		$16.7^{+19.3}_{-14.6}$	$1.37^{+0.08}_{-0.08}$	0.77/204
PKS 2126-158	~0.4–40	$10.4^{+3.1}_{-2.3}$	$1.63^{+0.07}_{-0.08}$	0.99/411
		116^{+84}_{-51}	$1.58^{+0.07}_{-0.06}$	1.01/411

Note: Intervals are at 90% confidence, for two interesting parameters.

[a] Approximate energy range, in the quasar rest frame.

B. Complex models for the absorption

Object	Warm Absorber (at z) + $N_{\rm Hgal}$				Broken Power Law ($N_{\rm H} \equiv N_{\rm Hgal}$)			
	$N_{\rm W}$ (cm^{-2})	Γ	ξ (ergs cm^{-2} s^{-1})	χ^2_{red}/dof	$\Gamma_{\rm soft}$	$E_{\rm break}$ (keV)	$\Gamma_{\rm hard}$	χ^2_{red}/dof
S5 0014+81	741^{+647}_{-298}	$1.72^{+0.09}_{-0.07}$	< 191	1.03/571	$-0.05^{+0.70}_{-1.51}$	$1.04^{+0.16}_{-0.12}$	$1.60^{+0.04}_{-0.04}$	1.03/571
NRAO 140	305^{+156}_{-124}	$1.72^{+0.05}_{-0.06}$	93^{+117}_{-76}	0.98/880	$0.85^{+0.12}_{-0.13}$	$1.57^{+0.11}_{-0.10}$	$1.64^{+0.05}_{-0.04}$	0.96/880
PKS 0438-436	213^{+292}_{-154}	$1.51^{+0.11}_{-0.11}$	< 100	0.99/280	<0.5	$0.68^{+0.37}_{-0.33}$	$1.41^{+0.08}_{-0.09}$	0.99/280
PKS 0537-286	216^{+820}_{-210}	$1.42^{+0.12}_{-0.12}$	< 4500	0.81/203	<1.32	<3.8	$1.47^{+0.37}_{-0.16}$	0.76/203
PKS 2126-158	398^{+552}_{-281}	$1.62^{+0.08}_{-0.07}$	< 455	1.01/410	$1.02^{+0.20}_{-0.27}$	$1.26^{+0.42}_{-0.26}$	$1.62^{+0.11}_{-0.07}$	1.00/410

Note: Intervals are at 90% confidence, for two interesting parameters.

C. Complex emission models

Object	Bremsstrahlung model (N_H free)			Reflection model (N_H free)			
	N_H (cm^{-2})	kT keV	χ^2_{red}/dof	N_H (cm^{-2})	Γ	R (=A_{refl}/A_{pl})	χ^2_{red}/dof
S5 0014+81	$18.73^{+3.71}_{-3.56}$	$42.1^{+8.00}_{-7.61}$	1.05/572	$27.8^{+7.5}_{-5.7}$	$1.75^{+0.25}_{-0.10}$	< 0.70	1.04/571
NRAO 140	$22.5^{+2.1}_{-2.5}$	$22.3^{+2.6}_{-2.3}$	0.99/881	$31.1^{+3.4}_{-1.5}$	$1.70^{+0.11}_{-0.05}$	< 0.35	0.98/880
PKS 0438-436	$4.63^{+1.68}_{-1.02}$	$52.7^{+30}_{-15.7}$	0.98/281	$5.86^{+6.21}_{-1.25}$	$1.49^{+0.26}_{-0.09}$	< 0.61	0.97/280
PKS 0537-286	$2.32^{+0.83}_{-0.60}$	89.7^{+75}_{-32}	0.80/204	$2.82^{+1.00}_{-0.72}$	$1.38^{+0.15}_{-0.08}$	< 0.35	0.81/203
PKS 2126-158	$6.90^{+1.53}_{-0.87}$	$41.9^{+10.0}_{-6.9}$	1.01/411	$10.4^{+3.9}_{-2.3}$	$1.62^{+0.26}_{-0.07}$	< 0.60	1.01/410

Note: Intervals are at 90% confidence, for two interesting parameters.

TABLE 7: Local Interstellar CO and IR Emission towards the Quasars

Object	l	b	CO[a] Emission ?	Ref.[b]	$IR^{c}_{100\mu m}$ Emission ?	Ref.[b]
S5 0014+81	121.6113	18.8020	possible	(1)	No	(6)
PKS 0332-403	244.7640	-54.0749	...	...	No	(6)
NRAO 140	158.9997	-18.7650	Yes	(2)	No	(6)
PKS 0438-436	248.4109	-41.5654	...	...	No	(6)
PKS 0537-286	232.9400	-27.2924	...	...	No	(6)
S5 0836+71	143.5408	34.4257	No	(3)	No	(6)
PKS 2126-158	35.9295	-41.8679	No	(4)	Yes	(6)
PKS 2149-306	17.0770	-50.7845	No	(5)	No	(6)

[a] An entry of "Yes"/"No" indicates ^{12}CO J=1–0 line Galactic emission has/hasn't been detected in the direction of the quasar (see §5.1.1.a).

[b] References: (1) Heithausen et al. (1993), (2) Bania et al. (1991), (3) Lisz & Wilson (1993), (4) Hartmann D., private communication, (5) Liszt (1994), (6) Moshir (1989)

[c] An entry of "Yes"/"No" indicates there is/isn't contamination by cirrus (see §5.1.1.a).

Fig. 1: χ^2 contour plots in the N_H–Γ parameter space. Full line contours represent 68%, 90% and 99% confidence limits obtained from *ROSAT* and *ASCA* (GIS+SIS). The 90% confidence contours obtained from fitting separately the GIS and SIS are indicated in dashed lines. Best-fit values are indicated by a large mark (+) for *ROSAT* and *ASCA* (GIS+SIS), and by a small mark (+) for GIS and SIS. The vertical line represent the Galactic absorption obtained from radio measurements at 21 cm with associated errors of 10^{19} cm^{-2} if taken from Elvis et al. (1989) or with a conservative 30% error, if taken from Dickey & Lockman (1990).

Fig. 2: Best-fit spectra and χ^2 contour plots of the combined *ROSAT* and *ASCA* data. The data are fitted with a single absorbed power law model, and have been binned to a S/N ratio higher than 4 for display purposes. Note that the *ROSAT* counts (lower spectra) have been normalized by the PSPC geometric area of 1141 cm^2. Therefore the *ROSAT* counts should be read as "normalized counts/sec/keV/cm^2". The contours represent the 68%, 90% and 99% confidence limits, and the vertical lines are, like in Fig. 1, the Galactic absorption and associated errors. For S5 0014+81, the energy of the Fe K edge has been indicated.

Fig. 3: X-ray photon indices vs. (a) redshift, (b) luminosity. Stars represent the *ASCA* slopes and errors between $\sim$ 1–30 keV (quasar frame) for the 8 high-z RLQs (Table 5, fit with N_H free). Triangles represent the *Ginga* slopes and errors between $\sim$ 2–20 keV for 18 low-z RLQs as reported by Lawson & Turner (1996). The horizontal shaded-line represents the approximate value $< \Gamma >= 1.4$ of the $\sim$ 2–10 keV slope of the XRB (Gendreau et al. 1995).

Fig. 4: χ^2 contour plots in the N_H–Γ parameter space for 3C 273. Full line contours represent 68%, 90% and 99% confidence limits for SIS0+1. Dashed lines indicate the 90% confidence contours for SIS0 chip number 1 (S0c1) and SIS1 chip number 3 (S1c3), fitted separately. Best-fit values are indicated with marks (+). The vertical line represent the Galactic absorption (full line) and associated 30% errors (dotted line) from Dickey & Lockman 1990.

?? Fig. 5: Histogram of the equivalent widths obtained with *Ginga* for a sample of Seyfert 1 galaxies (full line, Nandra & Pounds 1994) and upper limits obtained with *ASCA* for the present quasars (arrows).??

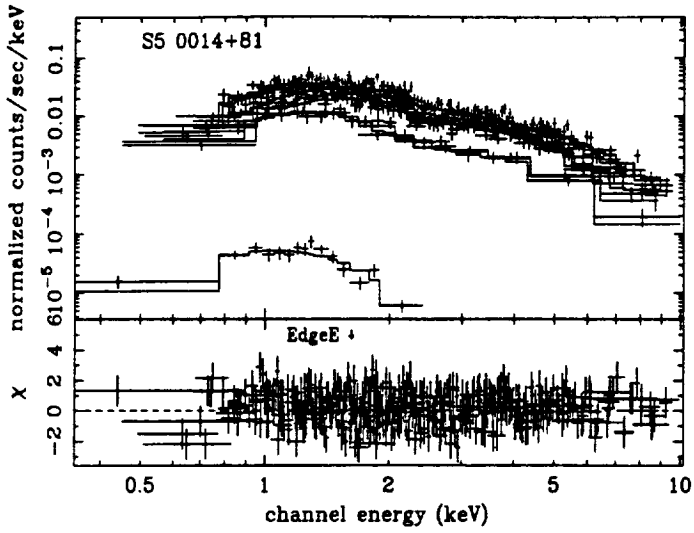
S5 0014+81
normalized counts/sec/keV
EdgeE
χ
channel energy (keV)

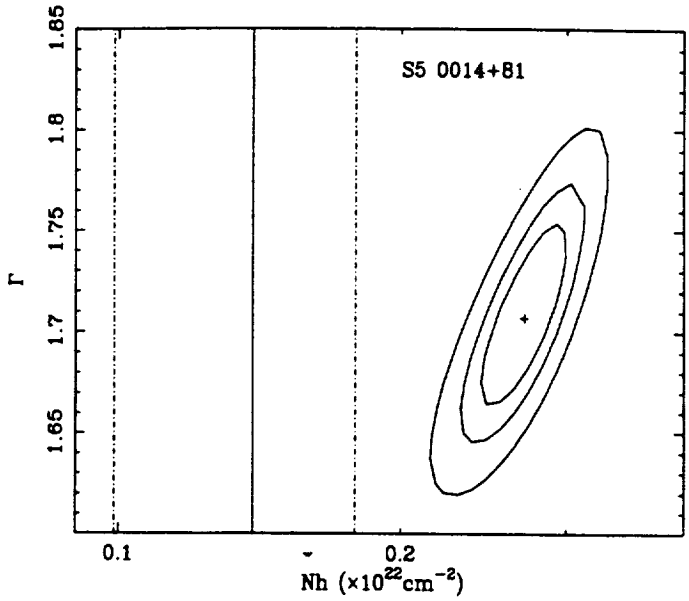
S5 0014+81
Γ
Nh (×10^22cm^-2)

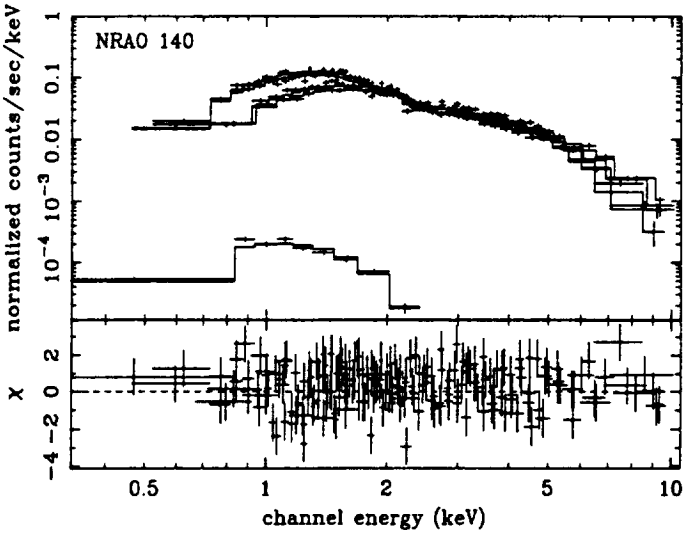
NRAO 140
normalized counts/sec/keV
χ
channel energy (keV)

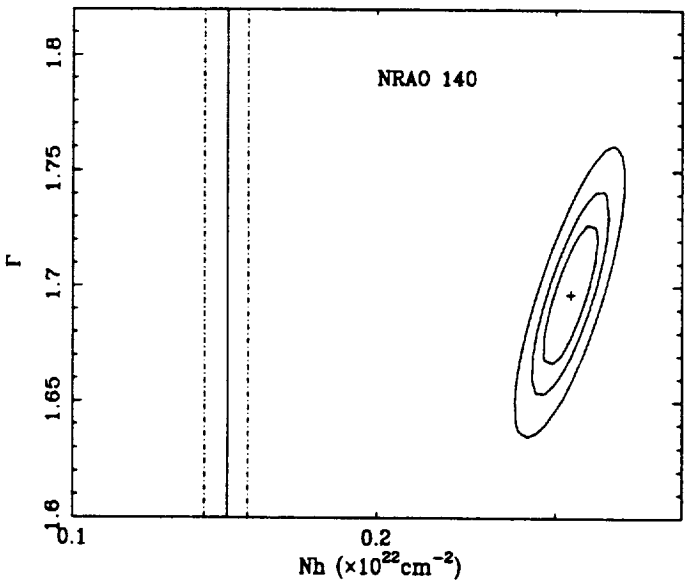
NRAO 140
Γ
Nh (×10^22cm^-2)

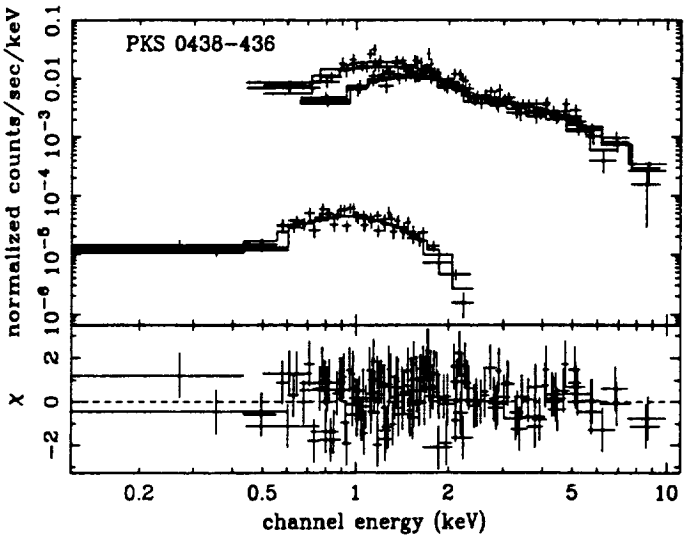
PKS 0438-436
normalized counts/sec/keV
χ
channel energy (keV)

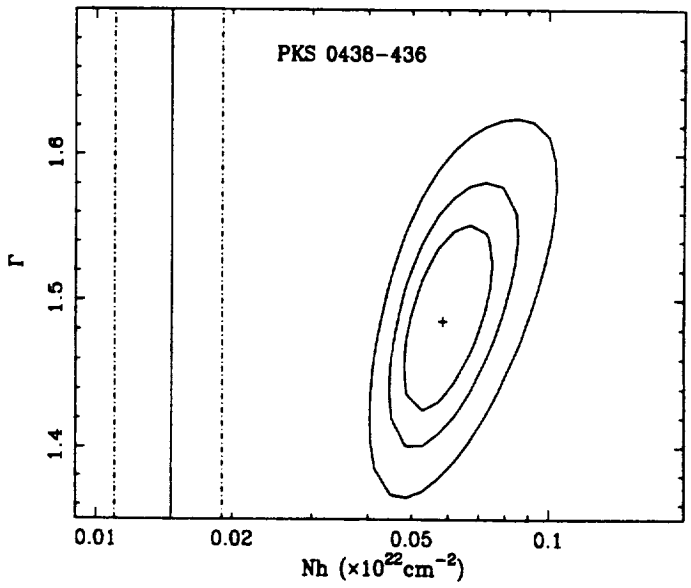
PKS 0438-436
Γ
Nh (×10^22cm^-2)

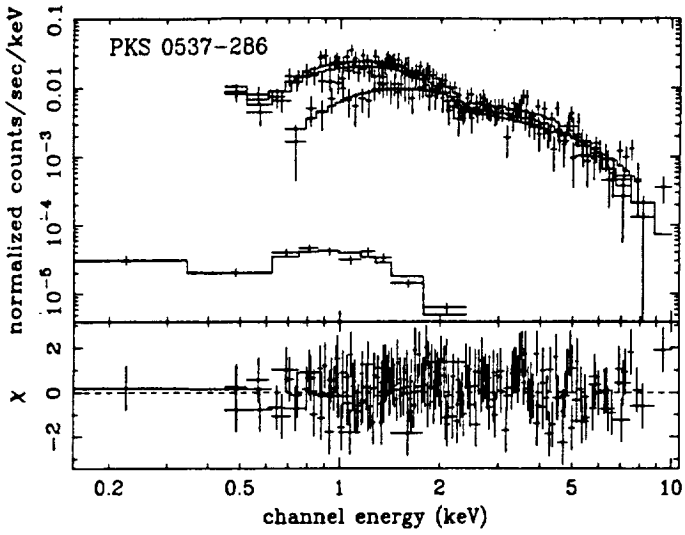
PKS 0537-286
normalized counts/sec/keV
χ
channel energy (keV)

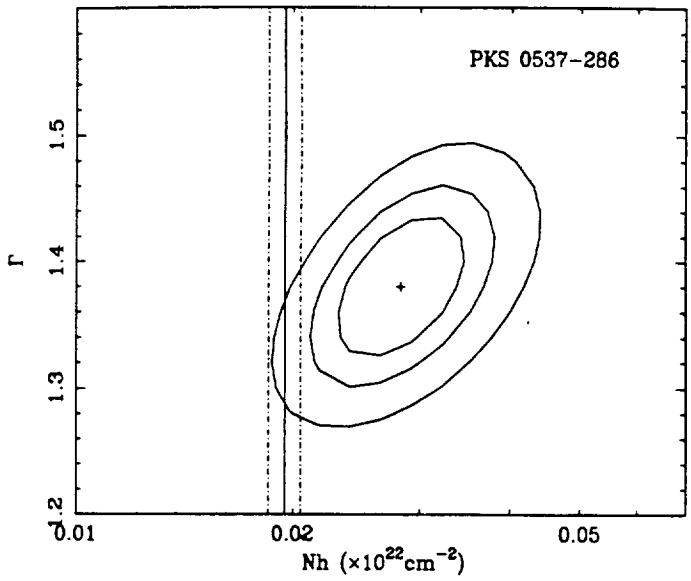
PKS 0537-286
Γ
Nh (×10^22cm^-2)

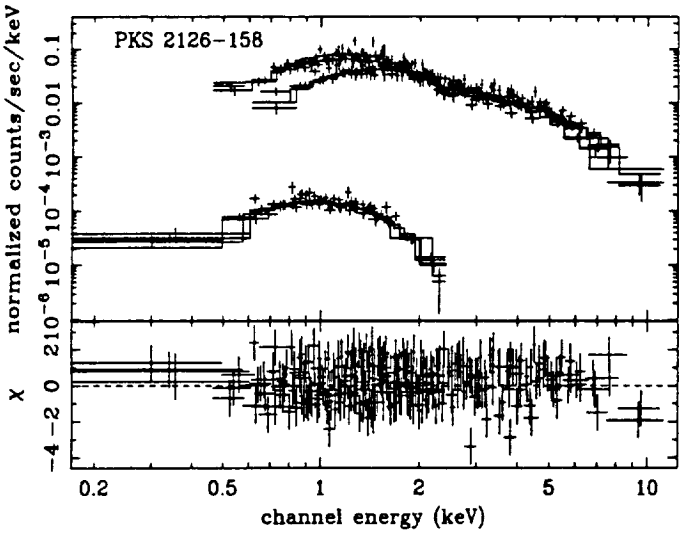
PKS 2126-158
normalized counts/sec/keV
χ
channel energy (keV)

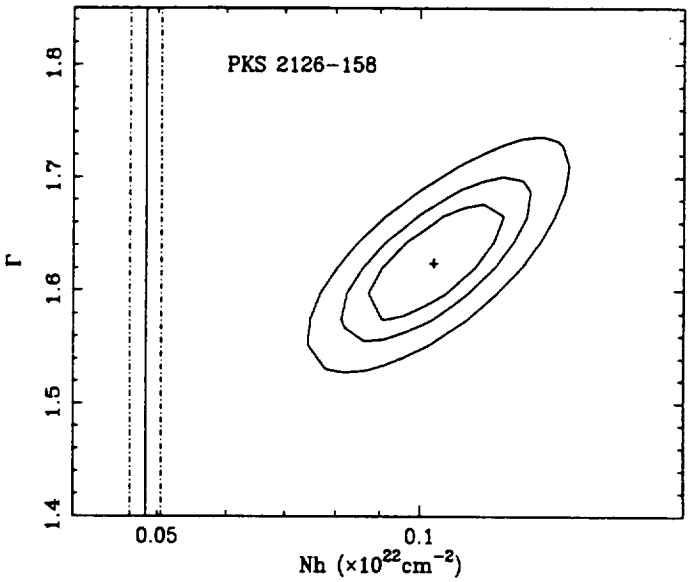
PKS 2126-158
Γ
Nh (×10^22cm^-2)

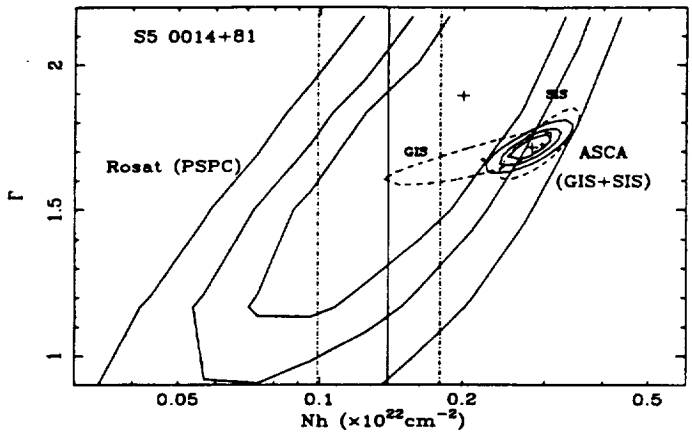
S5 0014+81
Rosat (PSPC)
ASCA
(GIS+SIS)
GIS
SIS
Γ
Nh (×10^22cm^-2)

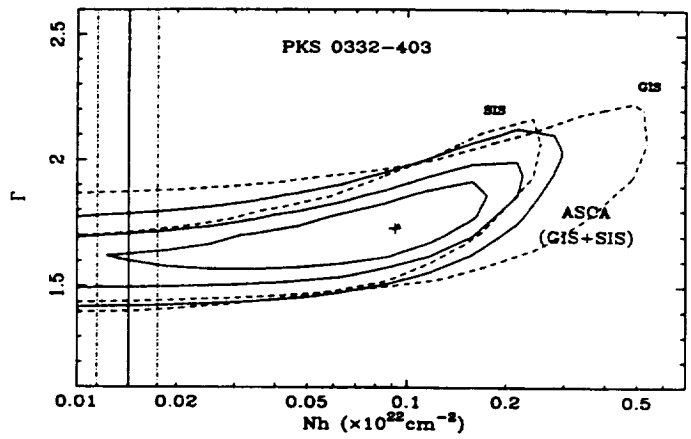
PKS 0332-403
ASCA
(GIS+SIS)
GIS
SIS
Γ
Nh (×10^22cm^-2)

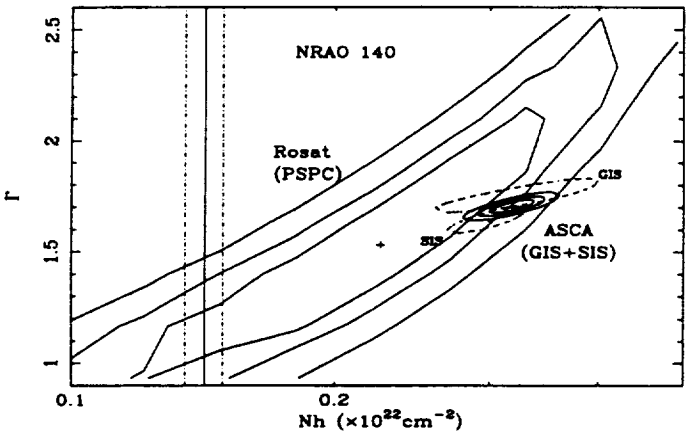
NRAO 140
Rosat
(PSPC)
ASCA
(GIS+SIS)
GIS
SIS
Γ
Nh (×10^22cm^-2)

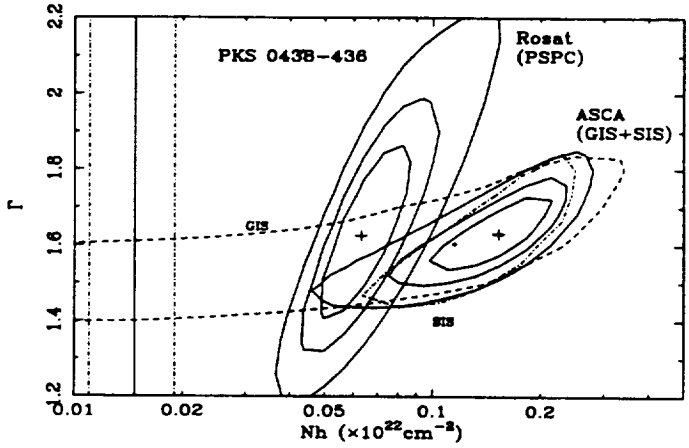
PKS 0438-436
Rosat
(PSPC)
ASCA
(GIS+SIS)
GIS
SIS
Γ
Nh (×10^22cm^-2)

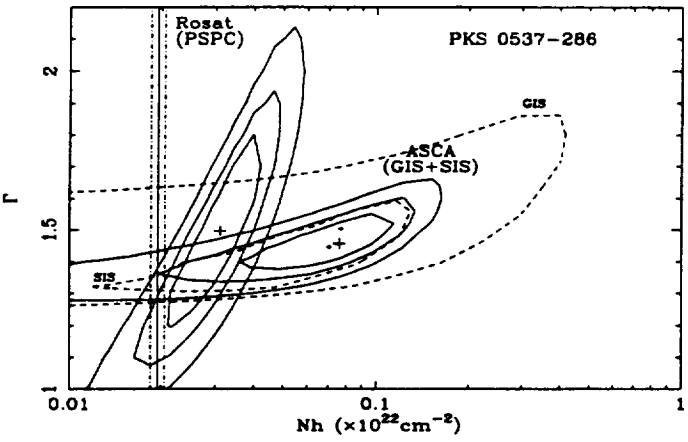
Rosat
(PSPC)
PKS 0537-286
ASCA
(GIS+SIS)
GIS
SIS
Γ
Nh (×10^22cm^-2)

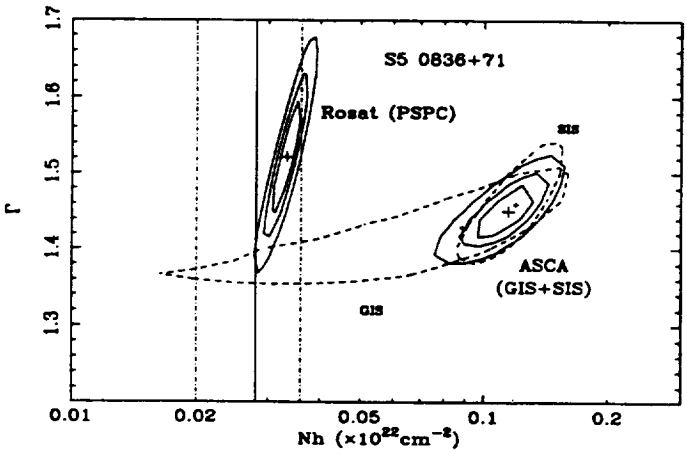
S5 0836+71
Rosat (PSPC)
ASCA
(GIS+SIS)
GIS
SIS
Γ
Nh (×10^22cm^-2)

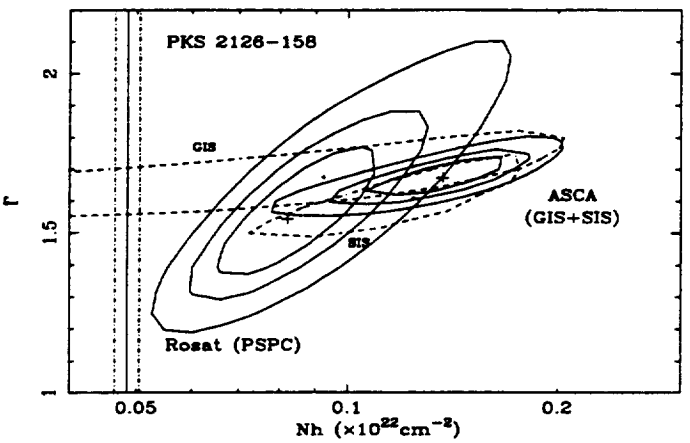
PKS 2126-158
GIS
ASCA
(GIS+SIS)
SIS
Rosat (PSPC)
Γ
Nh (×10^22cm^-2)

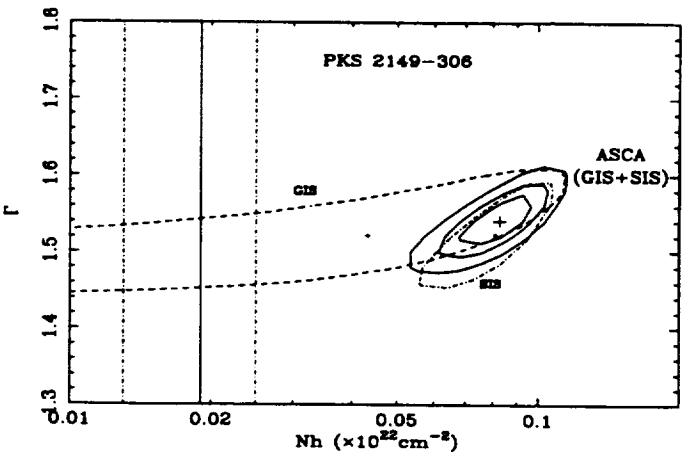
PKS 2149-306
ASCA
(GIS+SIS)
GIS
SIS
Γ
Nh (×10^22cm^-2)

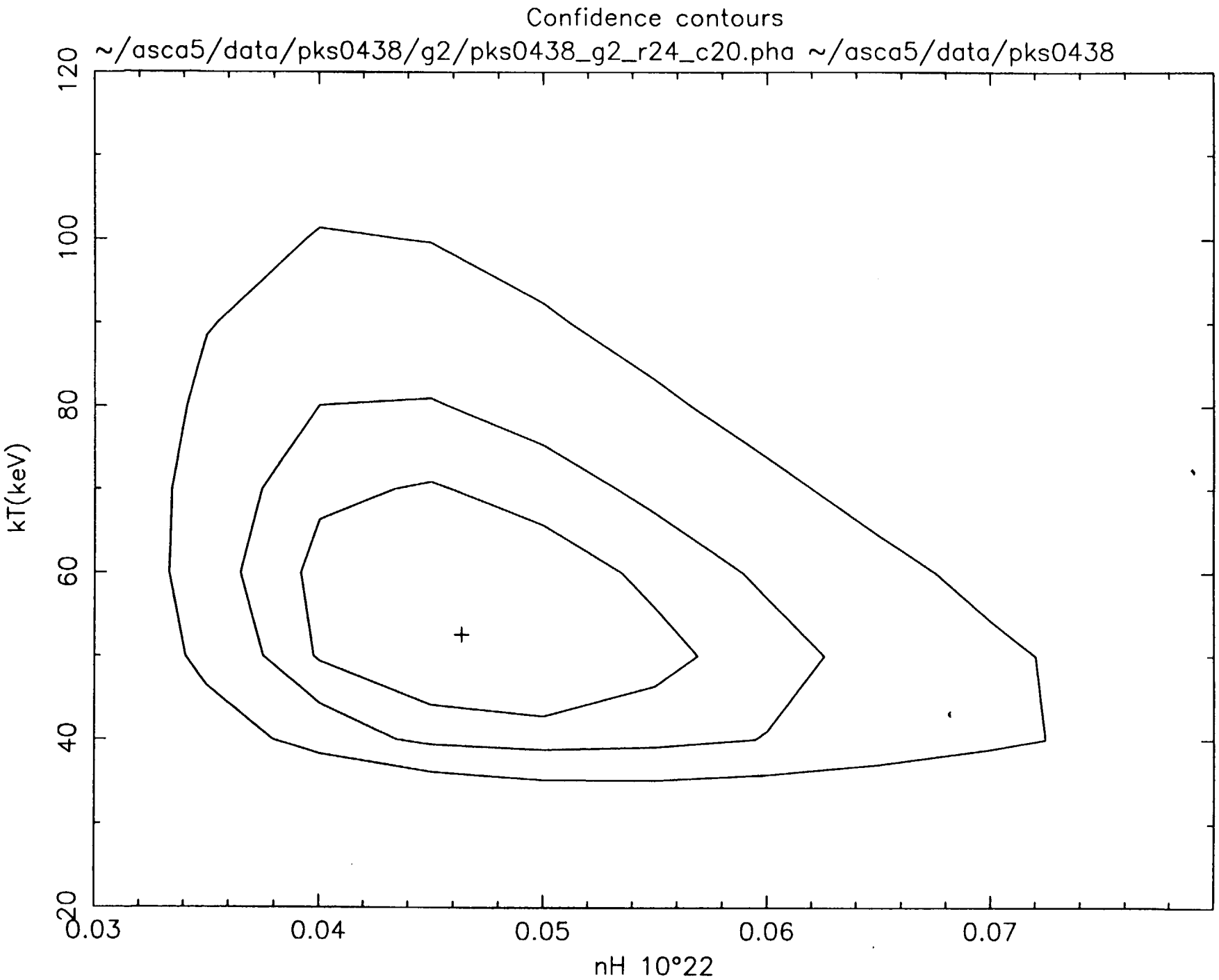

mcappi 1-Jun-1996 18:20

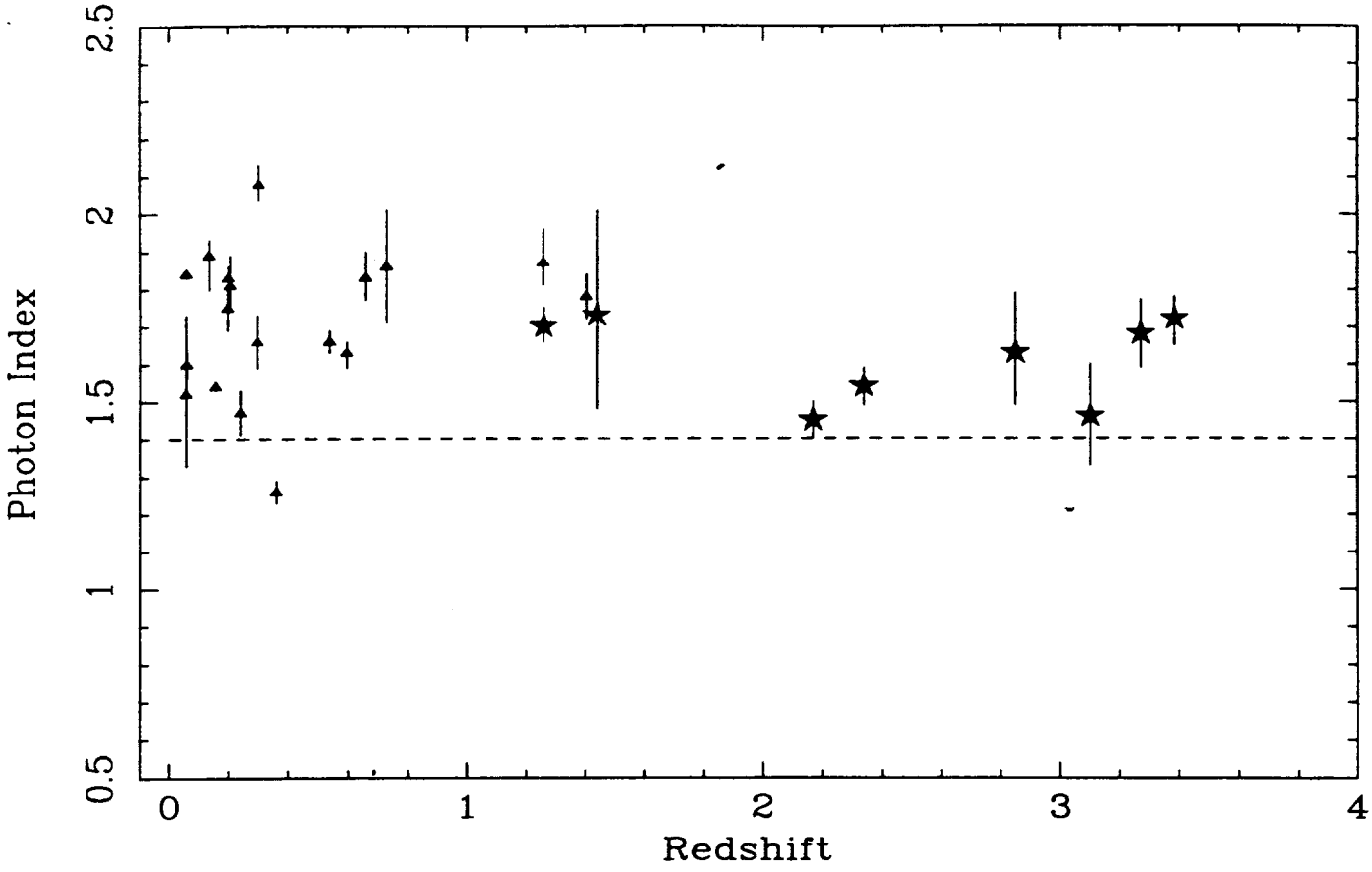
Photon Index
2.5
2
1.5
1
0.5
0
1
2
3
4
Redshift

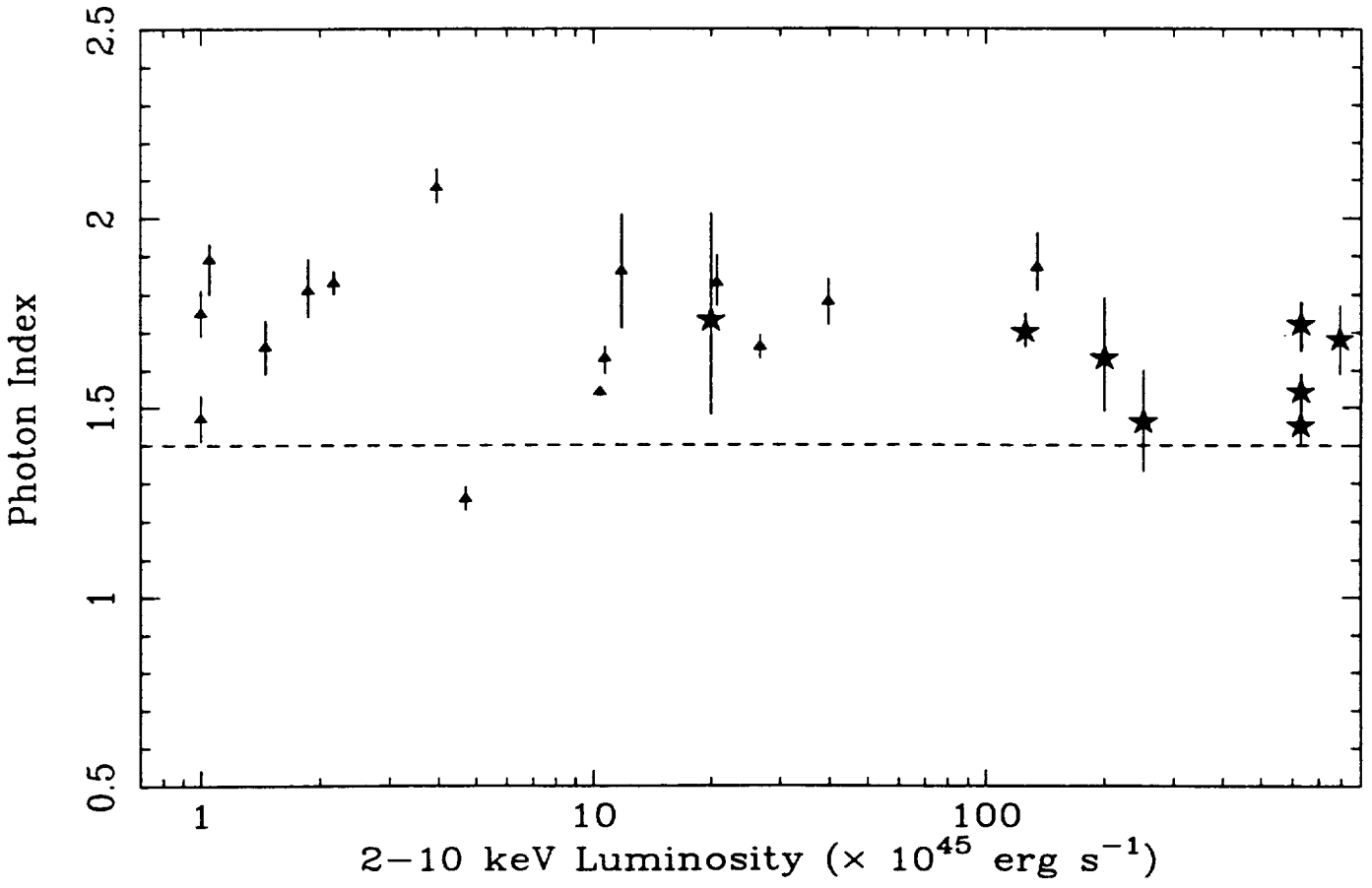
Photon Index
2.5
2
1.5
1
0.5
1
10
100
2−10 keV Luminosity (× 10^45 erg s^−1)

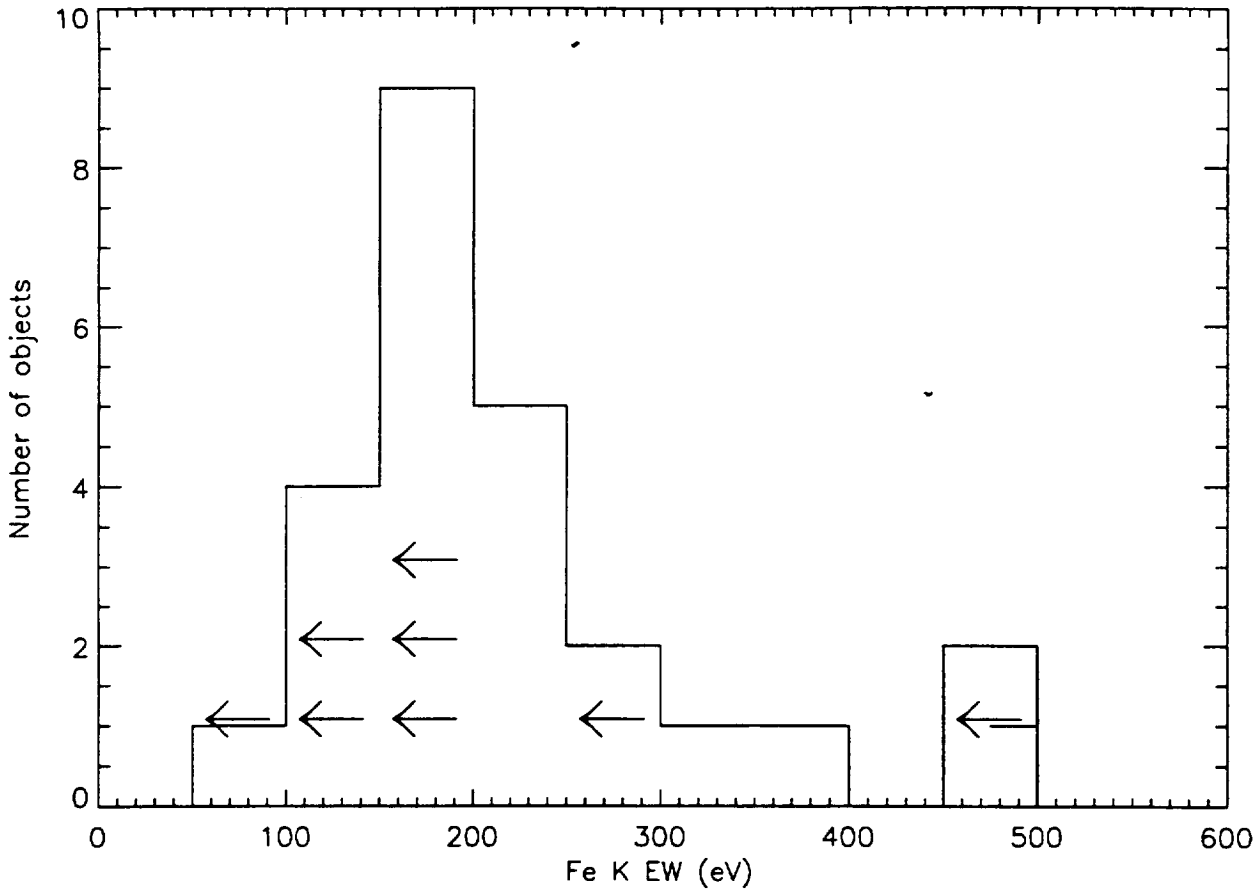
Number of objects
Fe K EW (eV)
0
2
4
6
8
10
0
100
200
300
400
500
600

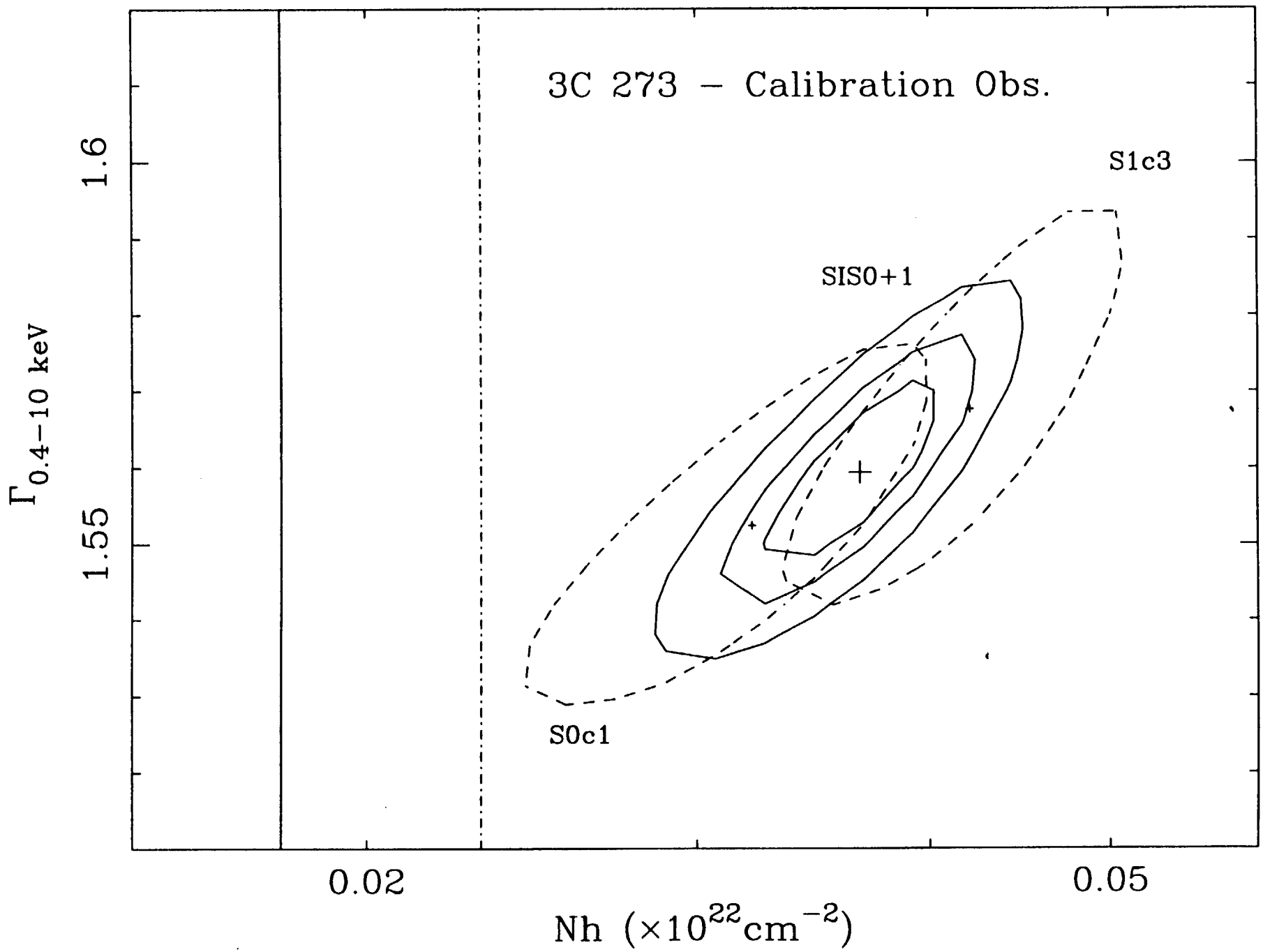
3C 273 – Calibration Obs.
S1c3
SIS0+1
S0c1
1.6
1.55
$\Gamma_{0.4-10\ keV}$
0.02
0.05
Nh ($\times 10^{22} cm^{-2}$)